AD-A043 959 TRW INC CLEVELAND OHIO F/G 11/2
ULTRASONIC INSPECTION OF CERAMICS CONTAINING SMALL FLAWS.(U)
MAR 77 T DERKACS, I M MATAY, W D BRENTNALL N62269-76-C-0148
UNCLASSIFIED TRW-ER-7867-F NL

OF
AD
A043959

END
DATE FILMED
10-77
DDC

ER-7867-F

13

B.S.

# ULTRASONIC INSPECTION OF CERAMICS CONTAINING SMALL FLAWS

T. Derkacs
I. M. Matay
W. D. Brentnall

TRW Inc.
Cleveland, Oh. 44117

MARCH 1977

Final Technical Report

Prepared Under Contract N62269-76-C-0148

NAVAL AIR DEVELOPMENT CENTER
WARMINSTER, PENNSYLVANIA 18974

FOR

NAVAL AIR SYSTEMS COMMAND
DEPARTMENT OF THE NAVY
WASHINGTON, D.C. 20361



Approved for public release; distribution unlimited.

SECURITY CLASSIFICATION OF THIS PAGE *(When Data Entered)*

## REPORT DOCUMENTATION PAGE

READ INSTRUCTIONS BEFORE COMPLETING FORM

| | |
|---|---|
| 1. REPORT NUMBER: (9) Final Technical Rept. 17 Feb 76 - 18 Feb 77 | 2. GOVT ACCESSION NO. / 3. RECIPIENT'S CATALOG NUMBER |
| 4. TITLE (and Subtitle): (6) ULTRASONIC INSPECTION OF CERAMICS CONTAINING SMALL FLAWS, (14) TRW-ER-7867-F | 5. TYPE OF REPORT & PERIOD COVERED: Final Technical Report, / 6. PERFORMING ORG. REPORT NUMBER |
| 7. AUTHOR(s): (10) Thomas Derkacs, Istvan M. Matay, William D. Brentnall | 8. CONTRACT OR GRANT NUMBER(s): (15) N62269-76-C-0148 |
| 9. PERFORMING ORGANIZATION NAME AND ADDRESS: TRW Inc. 23555 Euclid Avenue Cleveland, Ohio 44117 | 10. PROGRAM ELEMENT, PROJECT, TASK AREA & WORK UNIT NUMBERS: (11) Mar 77 |
| 11. CONTROLLING OFFICE NAME AND ADDRESS: Naval Air Systems Command Department of the Navy Washington, DC 20361 | 12. REPORT DATE: (12) 77 p. / 13. NUMBER OF PAGES: 72 |
| 14. MONITORING AGENCY NAME & ADDRESS *(if different from Controlling Office)*: Naval Air Development Center Warminster, Pa. 18974 | 15. SECURITY CLASS. *(of this report)* / 15a. DECLASSIFICATION/DOWNGRADING SCHEDULE |

16. DISTRIBUTION STATEMENT *(of this Report)*

Approved for public release; distribution unlimited.

17. DISTRIBUTION STATEMENT *(of the abstract entered in Block 20, if different from Report)*

18. SUPPLEMENTARY NOTES

19. KEY WORDS *(Continue on reverse side if necessary and identify by block number)*

Nondestructive Evaluation (NDE); ceramics; high frequency ultrasonics; flexural strength; hot pressed silicon nitride; hot pressed silicon carbide, sintered silicon carbide; flaws; fracture origins.

LESS THAN 100 MICRO M

20. ABSTRACT *(Continue on reverse side if necessary and identify by block number)*

A 45 MHz ultrasonic shear wave technique was developed and evaluated for detection of small defects, <100μm(0.004 inches), in gas turbine quality ceramics. Results for the shear wave technique were compared with the results for the previously developed 45 MHz longitudinal wave technique on hot pressed silicon nitride and silicon carbide from two vendors and on boron-doped sintered silicon carbide. Conventional mechanical tests were also performed to verify defect sizes and types and to correlate material

→ over

DD FORM 1 JAN 73 1473 EDITION OF 1 NOV 65 IS OBSOLETE
S/N 0102-014-6601

SECURITY CLASSIFICATION OF THIS PAGE *(When Data Entered)*

319550

strength with ultrasonic inspection results. The shear wave technique was found to have better sensitivity than the longitudinal wave technique, and specimens whose failure initiated at defects detected by the shear wave technique showed significantly lower strength than those whose cause of failure was undefined. Investigation of inspection frequencies up to 75MHz revealed the need for instrumentation and transducer performance improvements in order to achieve the potential for higher defect detection sensitivity.

## FOREWORD

This Final Technical Report describes the work performed for the Department of the Navy under Naval Air Development Center Contract N62269-76-C-0148 during the period 19 February 1976 to 18 February 1977. The work involved high frequency ultrasonic evaluation of ceramic materials, under the technical direction of Mr. Irving Machlin, AIR-52031B, Naval Air Systems Command, Washington, D. C. 20361.

This contract with the TRW Materials Technology Laboratory of TRW Equipment, TRW Inc., was carried out in the Materials Development Department, directed by Dr. I. J. Toth, Manager. TRW personnel contributing to this program, and their areas of involvement, were: Mr. I. M. Matay, Program Manager and instrumentation; Mr. T. Derkacs, Principle Investigator; and Mr. W. D. Brentnall, mechanical testing and metallography. Technical support to this program was provided by Mr. J. Touhalisky, ultrasonic inspections; Mr. C. A. Tyndall, mechanical testing; and Mr. W. G. Curtis, scanning electron microscope fractography.

This Final Technical Report has been given an internal TRW report number of ER-7867-F.

TABLE OF CONTENTS

## LIST OF ILLUSTRATIONS

LIST OF ILLUSTRATIONS (Cont'd)

## LIST OF TABLES

## LIST OF ABBREVIATIONS AND SYMBOLS

| Symbol | Quantity | Unit |
|---|---|---|
| Å | length | Angstrom |
| $Al_2O_3$ | aluminum oxide | - |
| b | specimen width | meter |
| C | temperature | Celsius |
| c | transducer distance from reference edge | meter |
| $c_1$ | c for defect detected by beam going down | meter |
| $c_2$ | c for defect detected by beam going up | meter |
| ° | temperature or angle | degree |
| d | depth of defect | meter |
| f | fundamental frequency of ultrasonic wave | hertz |
| g | mass | gram |
| Hz | frequency of oscillations per second | hertz |
| h | specimen height | meter |
| I | moment of inertia | quadric meter |
| IDS | hot pressed silicon nitride internal defect standard | - |
| K | stress intensity factor | newtons per square root of cubic meter |
| LDS | hot pressed silicon nitride laser drilled hole standard | - |
| l | specimen length | meter |
| $\lambda$ | ultrasonic wavelength | meter |
| M | moment | newton-meter |
| m | length | meter |
| MgO | magnesium oxide | - |
| min. | time | minute |
| $\mu$ | shear modulus | meganewtons per square meter |

| Symbol | Quantity | Unit |
|---|---|---|
| N | force | newton |
| P | force | newton |
| $\phi$ | angle of shear beam in material | degree |
| r | defect coordinate in direction of shear beam | meter |
| $\rho$ | density | grams per cubic centimeter |
| SEM | scanning electron microscope | - |
| $\sigma$ | Poisson's ratio | - |
| $\sigma_b$ | stress on specimen tensile surface | meganewtons per sq. meter |
| $\sigma_y$ | stress at defect location | meganewton |
| T | time of flight of ultrasonic beam | second |
| $T_1$ | time to defect located by beam going down | second |
| $T_2$ | time to defect detected by beam going up | second |
| t | billet thickness | meter |
| $\Theta$ | angle of incident ultrasonic beam | degree |
| $\Theta_L$ | angle of incident ultrasonic longitudinal wave | degree |
| $\Theta_s$ | angle of refracted ultrasonic shear wave | degree |
| $\Theta_1$ | angle of incident wave | degree |
| $\Theta_2$ | angle of refracted wave | degree |
| $V_L$ | ultrasonic longitudinal wave velocity | meters per second |
| $V_{L_w}$ | ultrasonic longitudinal wave velocity in water | meters per second |
| $V_1$ | wave velocity in medium 1 | meters per second |
| $V_2$ | wave velocity in medium 2 | meters per second |
| v | velocity of sound | meters per second |

LIST OF ABBREVIATIONS AND SYMBOLS (Cont'd)

| Symbol | Quantity | Unit |
|---|---|---|
| X | magnification | - |
| X | coordinate along billet edge | meter |
| x | distance from end of specimen | meter |
| Y | coordinate along billet edge | meter |

## PREFIXES

Decimal multiples and submultiples of the engineering units listed above are formed by means of the following prefixes:

| Symbol | Prefix | Multiplication Factor |
|---|---|---|
| M | mega | $10^{6}$ |
| K | kilo | $10^{3}$ |
| c | centi | $10^{-2}$ |
| m | milli | $10^{-3}$ |
| μ | micro | $10^{-6}$ |
| n | nano | $10^{-9}$ |

# 1.0 INTRODUCTION

The purpose of this program is to develop high frequency ultrasonic evaluation techniques capable of detecting defects in the 10 to 100 micrometer (μm) (0.0004 to 0.004 inch) range in gas turbine quality ceramics, such as silicon carbide and silicon nitride. Under a previous contract (Ref. 1) a high frequency (25-45 megahertz, MHz), longitudinal wave mode, pulse-reflection technique was developed and applied to a range of candidate gas turbine ceramics. This technique was shown to be capable of detecting voids at least as small as 25 μm (0.001 inch) and also high density inclusions, although of a somewhat larger size. It was also shown to be capable of detecting the porosity in a material that is not fully dense, such as reaction bonded silicon nitride. It was concluded in the previous program that, for fully dense material, an even higher inspection frequency is needed to allow detection of high density inclusions down to 10 μm (0.0004 inch). It was also concluded that shear wave inspection is needed to provide a correlation between ultrasonic inspection results and material flexural strength.

Effort under this contract, therefore, had two major objectives. One was to investigate ultrasonic inspection up to a frequency of about 75 MHz, within the limitations of present instrumentation. The other was to develop a shear wave inspection technique and to investigate the correlation of the inspection results with material flexural strength.

## 2.0 SUMMARY

Since the results of the previous program indicated that high frequency ultrasonics is best suited for ceramic materials that are close to theoretical density, effort in this program was concentrated on hot pressed materials. A billet of hot pressed silicon nitride and a billet of hot pressed silicon carbide were obtained from each of two vendors in the as-pressed condition. A small billet of boron-doped sintered silicon carbide was also included in the program.

Inspection frequencies up to 75 MHz were evaluated. However, due to the bandwidth-sensitivity characteristics of the available instrumentation and transducers, it was concluded that a frequency of 45 MHz provides the best results. Since instrument and transducer development were not within the scope of this program, development of higher frequency inspection was not pursued. It is strongly recommended, however, that both instrument and transducer development be carried out in order to achieve the potential of higher frequency inspection.

An ultrasonic shear wave technique was developed using two reference standards, one containing internal seeded defects which were characterized in the previous program and the other containing laser drilled holes. The technique employs a 45 MHz ultrasonic transducer with a 46 mm (1.8 inch) focal length in water used at a 10 mm (0.4 inch) water path at an angle of incidence of 10 to 11°. The billets were inspected both as received and after machining with a 320 grit diamond wheel to remove surface irregularities. It was found that these surface irregularities cause ultrasonic indications, but tend to inhibit detection of internal defects.

The program billets were inspected by both longitudinal and shear wave ultrasonic techniques and the results compared. The shear wave technique was found to detect many more defects than the longitudinal wave technique. A few defects were only detected by the longitudinal wave technique, however, apparently due to orientation. The billets of hot pressed silicon carbide were found to have very few defects and were not used for mechanical testing. The billet of sintered silicon carbide, of a type that has been well characterized by metallurgical evaluation, showed considerably more ultrasonic indications than expected.

Four-point-bend specimens were machined around defects detected only by the shear wave technique in the billets of hot pressed silicon nitride. Flexural strength measurements showed that those specimens, which initiated failure at ultrasonically detected defects, were significantly weaker than those with undefined, or multiple surface initiation sites. The ultrasonically detected defects that were failure initiation sites had major dimensions that ranged in size from 40 to 100 μm (0.0016 to 0.004 inch).

Investigation of the effectiveness of the shear wave technique for detecting artificial surface cracks indicated that difficulty is experienced in detecting defects less than 40 μm (0.0016 inch) deep. Results of mechanical testing supported this conclusion. It is recommended, therefore, that surface wave techniques be developed for this important type of defect.

In conclusion, the results of this program show that a 45 MHz ultrasonic shear wave technique has been successfully developed which is more sensitive than the previously developed longitudinal wave technique. The results also tend to support the theory that defects detected only by the shear wave technique are more likely to weaken the material, for the particular geometry of inspection and bend testing employed. Investigation of artificial surface cracks shows that development of surface wave techniques is warranted to achieve good sensitivity for this important type of defect.

## 3.0 MATERIALS

Under a previous contract (Ref. 1), it was determined that high frequency ultrasonics is best suited for the inspection of materials that are close to theoretical density. Therefore, the materials selected for this program are hot pressed silicon nitride and hot pressed silicon carbide which are close to theoretical density. Two billets of each material, one from each of two suppliers, were purchased to provide a comparison. A small billet of boron-doped, sintered silicon carbide was also inspected in this program. The following paragraphs describe each of these materials in more detail.

### 3.1 Hot Pressed Silicon Nitride

Billets of NC-132[+] and Ceralloy 147A[*] hot pressed silicon nitride were used in this program. The NC-132 was a 15 x 15 x 0.79 cm size billet of Norton's standard material with a manufacturer measured density of 3.28 g/cm$^3$. It was purchased in the as-pressed condition and came with a generally flat surface containing many small pits. Subsequent machining required the removal of 0.38mm from each side to remove the majority of the pits.

The Ceralloy 147A is made from 99 weight percent alpha-silicon nitride powder (AME[‡] CP85) and one percent MgO. The powder is ground for 72 hours in tungsten carbide and then hot pressed for two hours at 1750°C and 4000 psi (Ref. 2). The Ceralloy 147A was a 15 x 15 x 0.64 cm size billet with a manufacturer measured density of 3.32 g/cm$^3$. It was received with a generally smooth surface (no pits) containing some large scale irregularities including a deep crease along one edge. Subsequent machining required the removal of 0.25 mm from each side to eliminate all surface irregularities except the deep groove.

### 3.2 Hot Pressed Silicon Carbide

Billets of NC-203A[+] and Ceralloy 146A[*] hot pressed silicon carbide were used in this program. The NC-203A was a 15x15x0.79 cm size billet of Norton's standard material with a manufacturer measured density of 3.32 g/cm$^3$. It was purchased in the as-pressed condition and came with a generally good surface containing only a few small pits except for a bad spot near the center which was deeply pitted on both sides. Subsequent machining of 0.41 mm from each surface removed all surface irregularities except the bad area in the center. The Ceralloy 146A was used in the previous program (Ref. 1) where it was purchased already machined. It is 15 x 15 x 0.64 cm size and has a density of 3.24 g/cm$^3$. It is made from 98 weight percent silicon carbide and two percent $Al_2O_3$ (Ref. 2).

- - - - - - - - - - - - - - - - - - -

+ Norton Co., Worchester MA.
* Ceradyne, Inc., Chatsworth, California
‡ Advanced Materials Engineering, Ltd, Gateshead, Co. Durham, UK

## 3.3 Sintered Silicon Carbide

A 5.0 x 4.6 x 0.64 cm size billet of boron doped, sintered silicon carbide was provided for this program by the General Electric Co.* The material was cold pressed from beta-silicon carbide powder with small additions of boron and carbon and sintered at approximately 2100°C for 30 minutes. The final billet density was 93.5 percent of theoretical, and based on previous experience the billet was expected to contain a number of irregularly shaped pores with dimensions as large as 200 μm (Ref. 3).

## 3.4 Reference Standards

Two ultrasonic reference standards were used in this program. The first is a section of Ceralloy 147A billet 7.30 x 2.17 x 0.64 cm in size containing one seeded 125 μm low density ($Al_2O_3$) defect and one seeded 125 μm high density (WC) defect 2.5 cm apart (see Figure 1). This standard was left over from the previous program in which similar seeded defects were examined by scanning electron microscope (SEM) fractography (Ref. 1). This reference standard is called the internal defect standard (IDS), and appears in each of the C-scans of the program specimens.

The second reference standard is another section of Ceralloy 147A from the same billet as the IDS. The standard is 4.90 x 1.33 x 0.64 cm in size and contains eight laser drilled holes (see Figure 2) of various depths which are not known with any accuracy. Two of the holes were drilled at the edge to give an estimate of the typical cross-section. Figure 2 shows a) the layout of the holes and b) an 18X micrograph of the cross-section of the edge holes. The longer of the two edge holes is about 400 μm in diameter at the opening, but only 40 μm near the tip. Over the course of its 2600 μm depth, it increases in diameter by a factor of ten. The shorter hole is just as large at the surface and slightly smaller at the tip. The other six holes are about the same size at the opening, except for F which is only 125 μm. Holes F and H go all the way through the part. This reference standard is called the laser drilled standard (LDS) and appears in most of the shear wave C-scan recordings.

An attempt was also made to make a reference standard containing surface cracks. Petrovic, et al (Ref. 4) have shown that a Knoop microhardness tester will, under certain circumstances, produce a small surface flaw beneath the hardness indentation. A single flaw of this type on the tensile surface of a four-point bend specimen has a strong tendency to be the fracture initiation site. Furthermore, a fairly linear relationship exists between the size of the defect created and the indentation load. In hot pressed silicon nitride, surface flaws in the 20 to 80 μm range can be produced using a load in the 400 to 2800 g range. A small specimen of Ceralloy 147A left over from the previous program (Ref. 1) was surface polished successively using 9, 6 and 3 micron diamond paste. Knoop indentations were then made in the part using loads of 1,000, 700 and 500 g. The specimen was then inspected using the shear wave

- - - - - - - - - - - - - - - -

* G.E. R&D Center, Schenectady, N.Y.

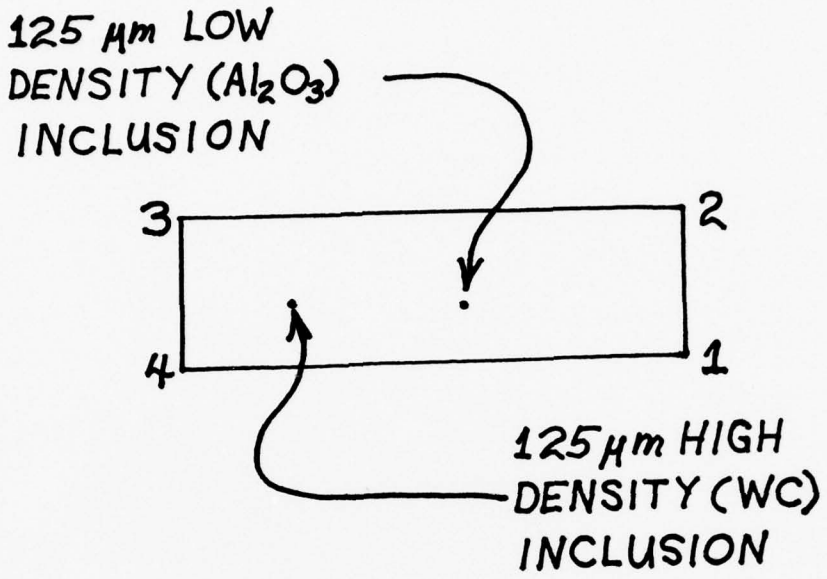


Figure 1. Layout of Ceralloy 147A, Hot Pressed Silicon Nitride Internal Defect Standard (IDS).

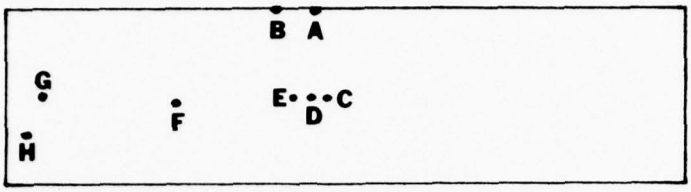


a. Layout of Laser Drilled Holes in Standard As Seen During Inspection (i.e., Holes Down).

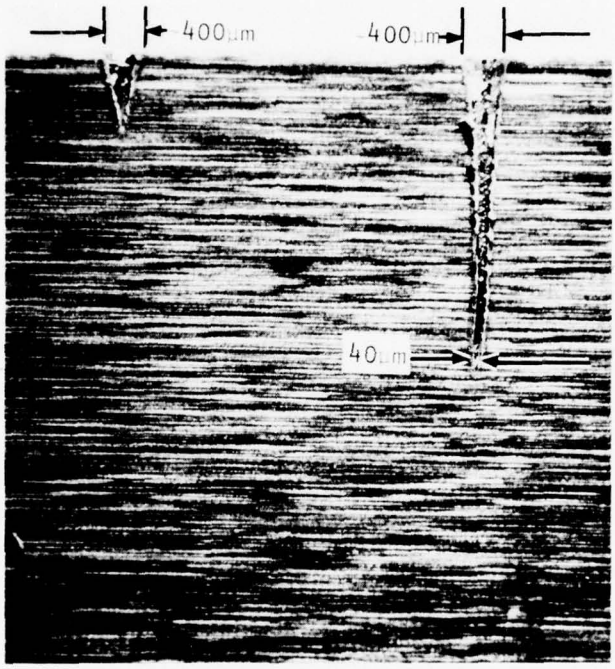


b. Photograph of Edge Holes Showing Typical Hole Profiles (18X).

Figure 2. Ceralloy 147A, Hot Pressed Silicon Nitride, Standard (LDS) Containing Laser Drilled Holes.

technique at 45 MHz with the cracks down. Although a slight signal could be observed on the A-scan display from the 1000 g load crack, the signal was too small to be recorded during C-scan inspection. Based on microscopic measurements of the indentation, this crack is about 70 microns across and is presumed to be about 35 microns deep. This specimen was not suitable as a surface flaw reference standard and was not used. The program schedule did not allow additional time to experiment with heavier loads to produce a useful reference standard by this method.

## 4.0 ULTRASONIC INSPECTION

In the previous program (Ref. 1) it was demonstrated that ultrasonic longitudinal wave inspection employing frequencies in the 25 to 45 MHz range is capable of detecting defects within the 10 to 100 μm range of interest in this program. Specifically, voids as small as 25 μm were verified metallurgically, and pulse height measurements from defects that were not verified metallurgically indicated that voids as small as 13 μm may have been detected. However, the need was also identified to detect smaller defects than this technique allows and to detect defects that are oriented perpendicular to the tensile loaded surface of a bend specimen. Two methods were employed in this program to achieve these goals. One approach was to use a higher ultrasonic frequency in order to be able to detect smaller defects. The other approach was to use shear wave inspection, both to detect smaller defects and to detect defects oriented perpendicular to the specimen surface.

### 4.1 Technical Background

Among the factors that affect the ability of ultrasonic waves to detect defects is the ultrasonic wavelength, $\lambda$. The wavelength must be at least of the same order of magnitude as the defect to be detected and preferably smaller. Yet it must be larger than the grain size of the material to avoid reflections from the individual grains of normal material structure which would cause high background noise and high attenuation. The frequency, f, of a sound wave in a material with acoustic velocity, v, is given by

$$f = \frac{v}{\lambda} \tag{1}$$

Therefore, one method that can be employed in an effort to detect larger defects is to increase the frequency, thereby reducing the wavelength.

#### 4.1.1 Shear Wave Generation

An ultrasonic beam traveling through a material can have several different modes of vibration, each with its own velocity of propagation. Among these are the longitudinal mode in which particles vibrate in the direction of wave propagation and the shear mode in which particles vibrate transverse to the direction of wave propagation. Although a liquid will not support a shear wave, when a longitudinal wave is incident at an angle other than normal to the interface between two materials, mode conversion generally occurs. Shear waves can therefore be generated in a material immersed in a liquid couplant by proper selection of the angle of incidence of the ultrasonic beam.

Figure 3 illustrates the relationship between an ultrasonic beam incident at the interface between two materials and the resulting refracted longitudinal and shear wave beams. The relationship between the incident and refracted beams is governed by the same law that applies in optics, Snell's law:

$$\frac{\sin\theta_1}{V_1} = \frac{\sin\theta_2}{V_2} \tag{2}$$

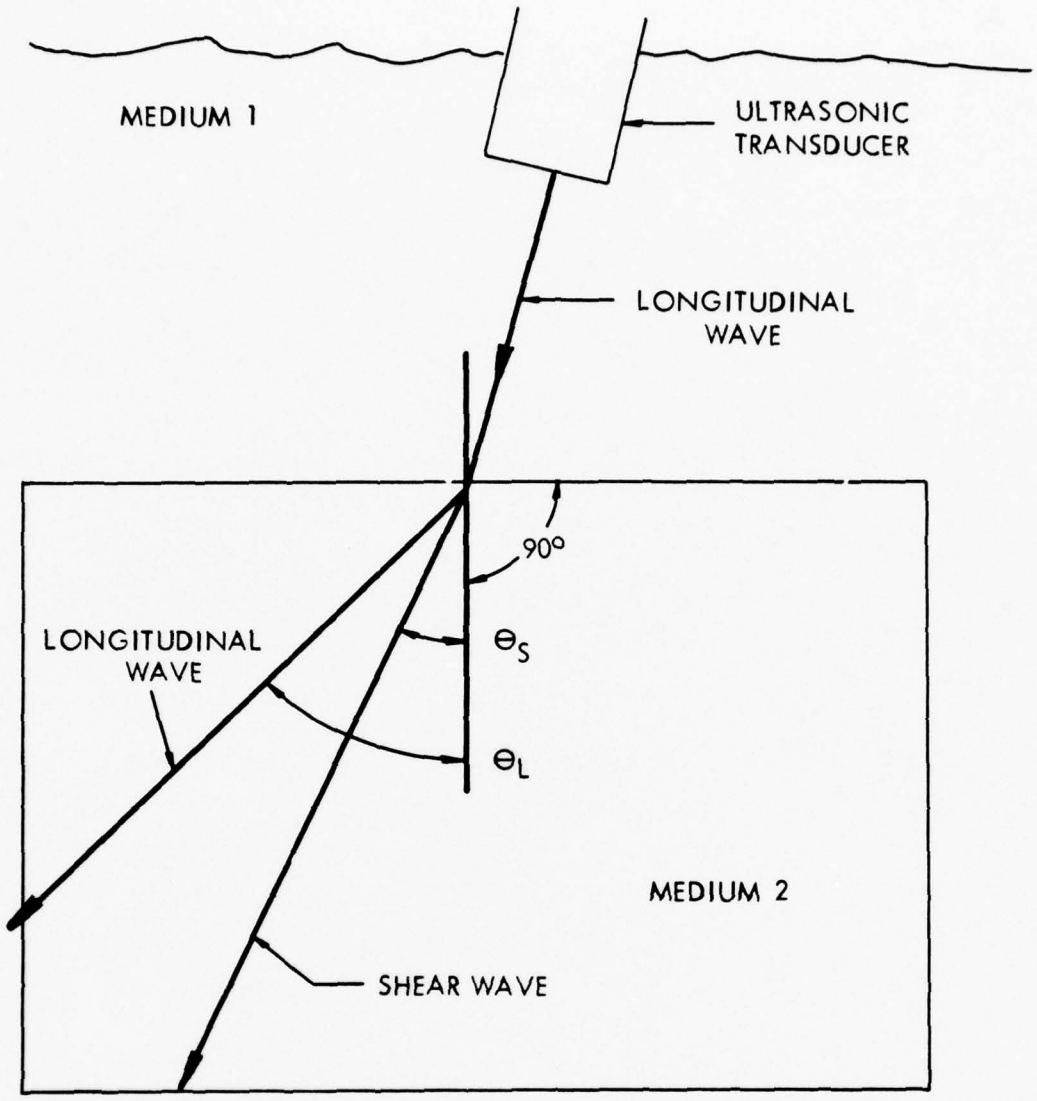


Figure 3. Illustration Showing Refraction of a Longitudinal Wave into Two Components.

where $\theta_1$ is the angle of incidence, $\theta_2$ is the angle of refraction and $V_1$ and $V_2$ are the acoustic velocities in media 1 and 2, respectively. The ratio between the longitudinal wave velocity, $V_L$, and the shear wave velocity, $V_S$, is given by:

$$\frac{V_L}{V_S} = \frac{1-2\sigma}{2(1-\sigma)} \tag{3}$$

Since $\sigma$, Poisson's ratio for the medium, is a number usually between zero and one, the shear velocity is less than the longitudinal velocity. It is therefore possible to select an angle of incidence such that $\theta_L$, the angle of refraction of the longitudinal wave in medium 2, is greater than 90°. As long as $\theta_S$, the angle of refraction of the shear wave, is less than 90°, only the shear wave will remain in the material.

The materials of interest in this program are hot pressed silicon carbide and silicon nitride, which are fully dense, and sintered silicon carbide with a density of about 3.0 g/cm$^3$. The longitudinal velocities for these materials were measured in the previous program. A review of the literature revealed no direct measurements of the shear velocities, however sufficient data was obtained to calculate the shear velocity. In addition to equation (2), the following relationship can be used to calculate the shear velocity:

$$V_S = \sqrt{\frac{\mu}{\rho}} \tag{4}$$

where $\mu$ is the shear modulus of a material of density, $\rho$. Table I lists a number of values of Poisson's ratio, the shear modulus and the density for the three materials of interest along with corresponding shear velocities and minimum and maximum angles of incidence.

Since the velocities of shear waves in the materials of interest in this program are on the order of sixty percent of the longitudinal wave velocities, another method that can be employed to reduce the ultrasonic wavelength by almost a factor of two with no increase in frequency, is to substitute shear wave inspection for longitudinal wave inspection. Furthermore, inserting values from Table I into Equation (2) reveals that the angle of the beam inside the material is on the order of 45°. Therefore, shear wave inspection has a much higher probability of detecting defects oriented perpendicular to the surface, such as cracks.

### 4.1.2 Measurement of Ultrasonic Shear Velocity

Figure 4 shows a setup for measuring the velocity of sound in a ceramic billet of thickness, t. In this figure, $\theta$ is the angle of incidence of the beam, $\phi$ is the angle of the refracted shear wave and c is the distance from the edge of the billet to where the beam strikes the top surface. The

TABLE 1

CALCULATED SHEAR VELOCITIES AND CORRESPONDING ANGLES OF INCIDENCE FOR VARIOUS CERAMIC MATERIALS

| Material and Source | Poisson's Ratio $\sigma$ | Shear Modulus $\mu$ ($MN/m^2$) | Density ($g/cm^3$) | Shear Velocity (m/s) | Angle of Incidence Min. (degree) | Angle of Incidence Max. (degree) |
|---|---|---|---|---|---|---|
| Hot Pressed $Si_3N_4$ | | | | | | |
| Ref. 5 (HS-110) | 0.26 | $1.20 \times 10^5$ | 3.33 | 5980 (1) | 8.2 | 14.4 |
| | | | | 6000 (2) | 8.2 | 14.4 |
| | 0.27 | $1.20 \times 10^5$ | 3.20 | 5890 (1) | 8.2 | 14.7 |
| | | | | 6120 (2) | 8.2 | 14.1 |
| Ref. 6 | - | $1.18 \times 10^5$ | 3.18 | 6090 (2) | 8.2 | 14.2 |
| Hot Pressed SiC | | | | | | |
| Ref. 7 | 0.173 | - | 3.141 | 7700 (1) | 7.0 | 11.2 |
| | 0.174 | - | 3.035 | 7700 (1) | 7.0 | 11.2 |
| Ref. 6 | - | $1.97 \times 10^5$ | 3.28 | 7740 (2) | 7.0 | 11.1 |
| Sintered SiC | | | | | | |
| Ref. 7 | 0.186 | - | 3.103 | 6630 (1) | 8.0 | 13.0 |

(1) Shear velocity calculated from Poisson's ratio and assumed longitudinal wave velocity of 10500 m/s for hot pressed silicon nitride, 12250 m/s for hot pressed silicon carbide, and 10670 m/s for sintered silicon carbide.

(2) Shear velocity calculated from density and shear modulus.

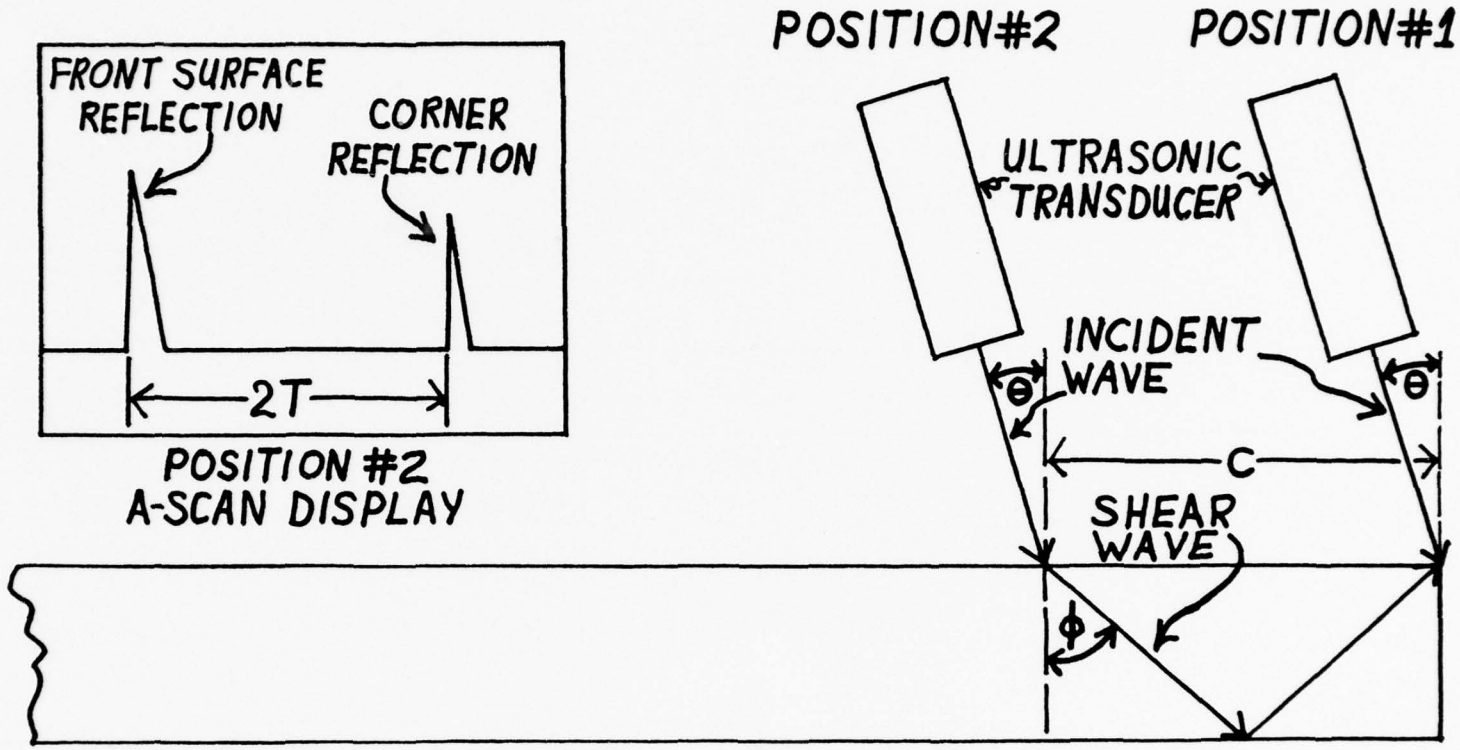


Figure 4. Technique for Measurement of Ultrasonic Shear Wave Velocity.

measurement technique consists of aligning the transducer in position #1 so that the beam just strikes the top corner of the billet, then moving the transducer to position #2 where the beam strikes the top corner after reflection from the bottom surface. Measurement of the distance of transducer travel, c, and the time of flight of the ultrasonic beam, T, in position #2 can then be used to find $\phi$, the shear velocity, $V_S$, and $\theta$ from the following equations:

$$\phi = \tan^{-1}\left(\frac{c}{2t}\right) \tag{5}$$

$$V_S = \frac{2t}{T\cos\phi} \tag{6}$$

$$\text{and } \theta = \sin^{-1}\left(\frac{V_{L_W}\sin\phi}{V_s}\right) \tag{7}$$

Where $V_{L_W}$ is the longitudinal sound velocity in water. The angle of incidence, $\theta$, is, of course, set by the operator, but this technique allows an accurate calculation to be made of the actual beam angle.

### 4.1.3 Location of Defects Detected by Shear Wave Inspection

In order to make fluxural strength specimens containing ultrasonically detected flaws near the tensile surface, it is necessary to make accurate determinations of defect locations. While the C-scan recording presents a two-dimensional picture of defect locations, it provides indications that are much larger than the actual defect size, therefore introducing uncertainty as to the actual defect location. Also, hysteresis in the scanning system used in these tests introduces additional uncertainty. These uncertainties are not significant in the inspection of metals, where relatively large defects must be detected. For locations of very small defects in ceramics, however, they represent a serious problem. For longitudinal wave inspection, defects were located by obtaining the peak defect signal and then marking the outline of the transducer on the part. The defect was then assumed to be at the center of the transducer. It was hoped by this method to locate defects within ±0.38 mm. Based on the results of the flexural strength testing, however, it seems unlikely that this accuracy was achieved.

Even if the technique used for longitudinal wave inspection were sufficiently accurate, it is not applicable for shear wave inspection because the transducer is not located directly over the defect. Therefore, the following scheme has been worked out to locate defects detected by shear wave inspection.

Having accurately determined the shear velocity in the material and the angle of beam incidence, the same setup can then be used to measure defect locations as shown in Figure 5. Once again the edge of the billet is used for a reference. In this case, however, the defects can be viewed either from position #2 or position #3 or both. In position #3 the beam strikes the defect after reflection from the bottom surface. The two coordinates that define the defect location in the plane shown are d, the depth from the top surface, and r, the distance from the reference edge of the billet. The measurement technique is to position the transducer at the point of maximum signal response from the defect and then measure c and T. T is, of course, measured from the A-Scan display of an oscilloscope. The defect coordinates are then given by the following equations:

a) Defect detected by beam going down:

$$d = V_s \, T \cos\phi \tag{8}$$

b) Defect detected by beam going up (reflected from bottom surface):

$$d = 2t - V_s \, T \cos\phi \tag{9}$$

c) Defect detected by both methods:

$$d = t - \frac{c_2 - c_1}{2 \tan\phi} \tag{10}$$

$$\text{or } d = t - \frac{V_s \, (T_2 - T_1) \cos\phi}{2} \tag{11}$$

and for all the above cases

$$r = c - V_s \, T \sin\phi \tag{12}$$

In Equations (10) and (11), the subscripts 1 and 2 refer to measurements made with the beam going down and up, respectively. In Equation (12) either $c_1$ and $T_1$ or $c_2$ and $T_2$ may be used for the case where defects are detected by both methods.

These equations provide the values d and r which can conveniently be used to locate defects from a reference edge for machining. The third coordinate is the distance of the transducer from the side edge of the part.

## 4.2 Higher Frequency Ultrasonic Inspection

A 75 MHz broadband delay type ultrasonic transducer was procured for this program. It has a 6.4 mm diameter element and a fused silica delay line sized to allow operation at up to a 12.7 mm water path. The end of the delay line is machined to provide a focal length of 50 mm in water. The spectrum analysis provided with the transducer indicates a significant output over a range of 45 to 75 MHz with a sharp peak at about 68 MHz.

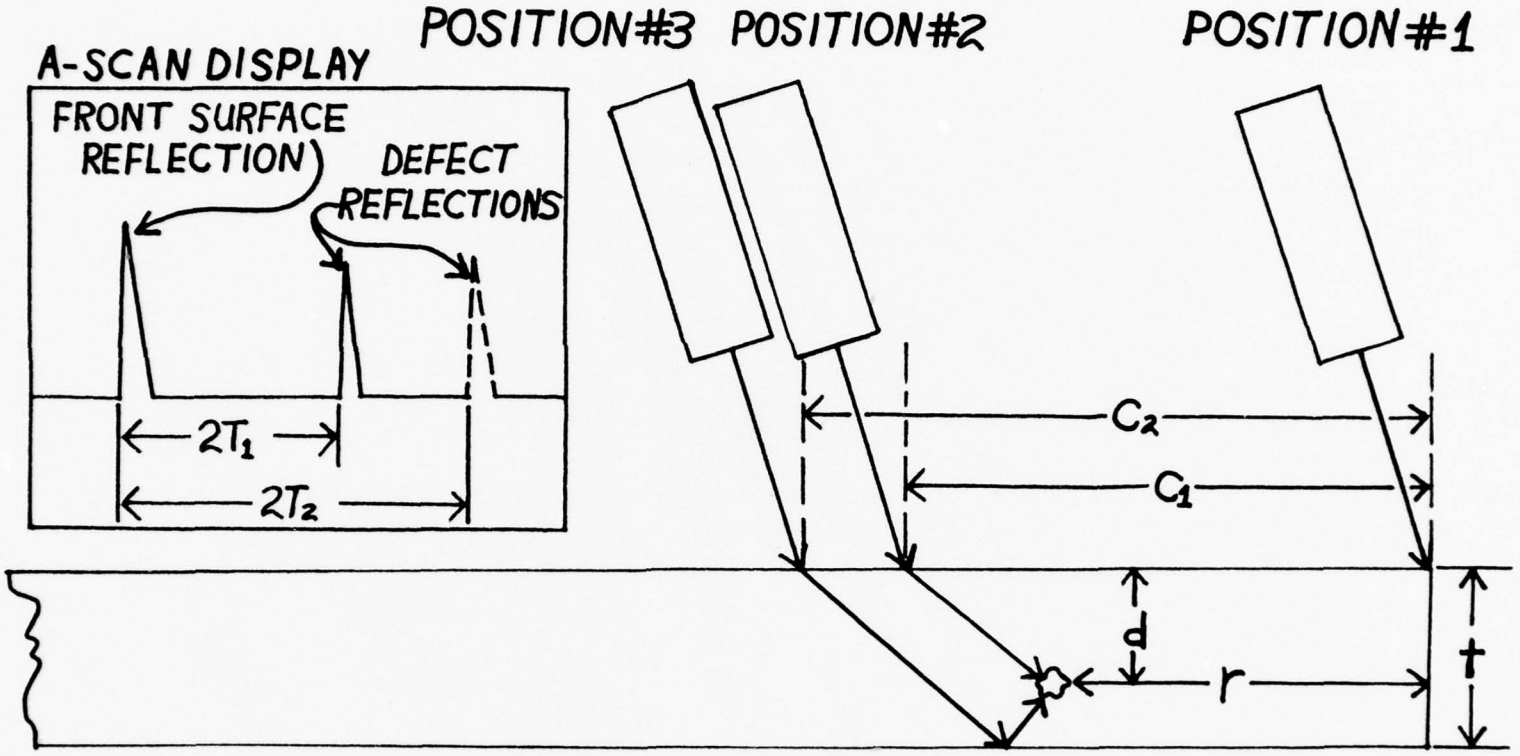


Figure 5. Technique for Determining the Location of Defects Detected by Ultrasonic Shear Wave Inspection.

This transducer was connected to the existing instrumentation and an effort was made to detect the seeded defects in the IDS. This was totally unsuccessful. The number of back surface reflections observed on the A-scan display was considerably less than with the 45 MHz transducer indicating considerably reduced sensitivity. It was concluded that either the transducer is not as sensitive or the bandwidth of the receiver is not adequate to achieve good sensitivity at the frequency of operation of the transducer, or most likely both. Since instrument development was not within the scope of this contract, no attempt was made to improve the instrument bandwidth.

## 4.3 Shear Wave Inspection

The major goal of the ultrasonic inspections was to identify defects that could be detected by shear wave inspection, but not by longitudinal wave inspection. Such defects are expected to be oriented perpendicular to the billet surface and therefore to have the highest stress concentration when a surface parallel to the billet surface is used as the tensile surface of a four-point-bend specimen. In order to determine such defects each of the billets, except the sintered silicon carbide, was first thoroughly inspected using the longitudinal wave technique developed in the previous program and then by the shear wave technique. The longitudinal wave inspection consisted of three scans, one focused at the centerplane of the billet and one focused near each surface from the opposite side. The shear wave inspection consisted of four scans, two from each side of the billet oriented 90° apart and focused near the opposite surface. The two orientations were required to detect defects of different orientations and also to cover the deadband which occurs along one edge of a part during shear wave inspection. The focal length used was selected because it was found that the seeded defects in the IDS could be detected, even though the transducer was not focused at the centerplane of the billet.

A secondary goal of these inspections was to determine the effect of surface finish on inspection results. Therefore, the billets that were purchased new for this program, the NC-132, NC-203A and Ceralloy 147A were purchased as pressed. A few initial inspections were performed and then the billets were machined to clean up the surface using a 320 grit diamond wheel. In the case of the NC-132 and NC-203A, a 220 grit diamond wheel was used for rough machining and then the 320 grit wheel was used to provide the final surface finish.

Early in the program a shear wave technique was used in which the ultrasonic defect gate width was set to be equal to the time required for the beam to travel from the top surface to the bottom surface of the billet. This technique successfully detected the defects in the IDS and created only a small deadband. However, this technique could not detect the laser drilled holes in the LDS. When the gate width was doubled the laser drilled holes were detected but the deadband was also doubled. Inspection of the billet of Ceralloy 147A by both techniques showed that the double gate width also allowed detection of more naturally occurring defects. Therefore, all of the final shear wave inspection were accomplished using the double gate width technique.

The following sections present the results of the various ultrasonic inspections and the conclusions that can be drawn from these results. In each C-scan recording presented the corners of the billets and the IDS are numbered to show orientation. In the shear wave scans the lines drawn by the stylus are parallel to the direction in which the transducer was tilted. Since the C-scan recorder tends to enlarge indications in the direction of scan, the large dimension of a defect is likely to be perpendicular to the large dimension of the indication. This can only be determined for certain by comparing the results of two scans made 90° apart. In addition, some of the particularly long indications are caused by the fact that some defects are detected twice; once when the beam is going down and again after reflection off the bottom surface. If the defect is close to the bottom these two indications may be connected to make one long indication. It should also be noted that indications in a C-scan recording can be caused by real defects within the gate, by surface anomalies that cause the defect gate to shift into an interface pulse, or by random reflected ultrasonic waves or electrical noise. Most of the indications seen in the unmachined billets, for example, are caused by shifting of the defect gate. On a C-scan recording of a machined billet indications which consist of more than one adjacent line (usually offset slightly because of hysteresis) are caused by defect pulses within the gate. Small defects on the top surface as well as ultrasonic or electrical noise usually cause short, single lines. Short, single lines are also caused, however, by very small defects. The only way to differentiate is to examine the A-scan display on the oscilloscope or to compare successive scans for indications that appear repeatedly from different orientations or from different sides of the billet. It was not necessary to fulfill the program objective to examine all of the indications of this type that were found on the many C-scan recordings made in this program. Nevertheless, of the ones that were examined, the majority were found to be real defects. These factors should be considered in interpreting the results of the shear wave inspections.

### 4.3.1 Effect of Surface Finish

Figures 6 through 13 show some typical C-scan recordings that illustrate the results observed for the materials that were inspected before and after surface machining. Figures 6 and 7 are C-scan recordings of the Ceralloy 147A at 45 MHz using an 11° angle of incidence. The single gate width technique was used. In these two figures four indications are labelled with the letter D indicating that they are internal defects that appear in both scans. All the other indications in Figure 6 are due to surface defects. The other indications in Figure 7 are mostly internal defects that were not previously detected. Some are defects in the new surface. Figures 8 and 9 are C-scan recordings of ultrasonic longitudinal wave inspections of NC-132 at 45 MHz before and after machining. Figure 8 shows extensive areas of surface related indications caused by pitting. In Figure 9, the one internal defect detected is labelled D. The other indications are caused by flaws in the new surface. Figures 10 through 13 are C-scan recordings of longitudinal and shear wave inspections of the NC-203A at 45 MHz before and after machining. This billet had an area of surface porosity near the center on both sides before

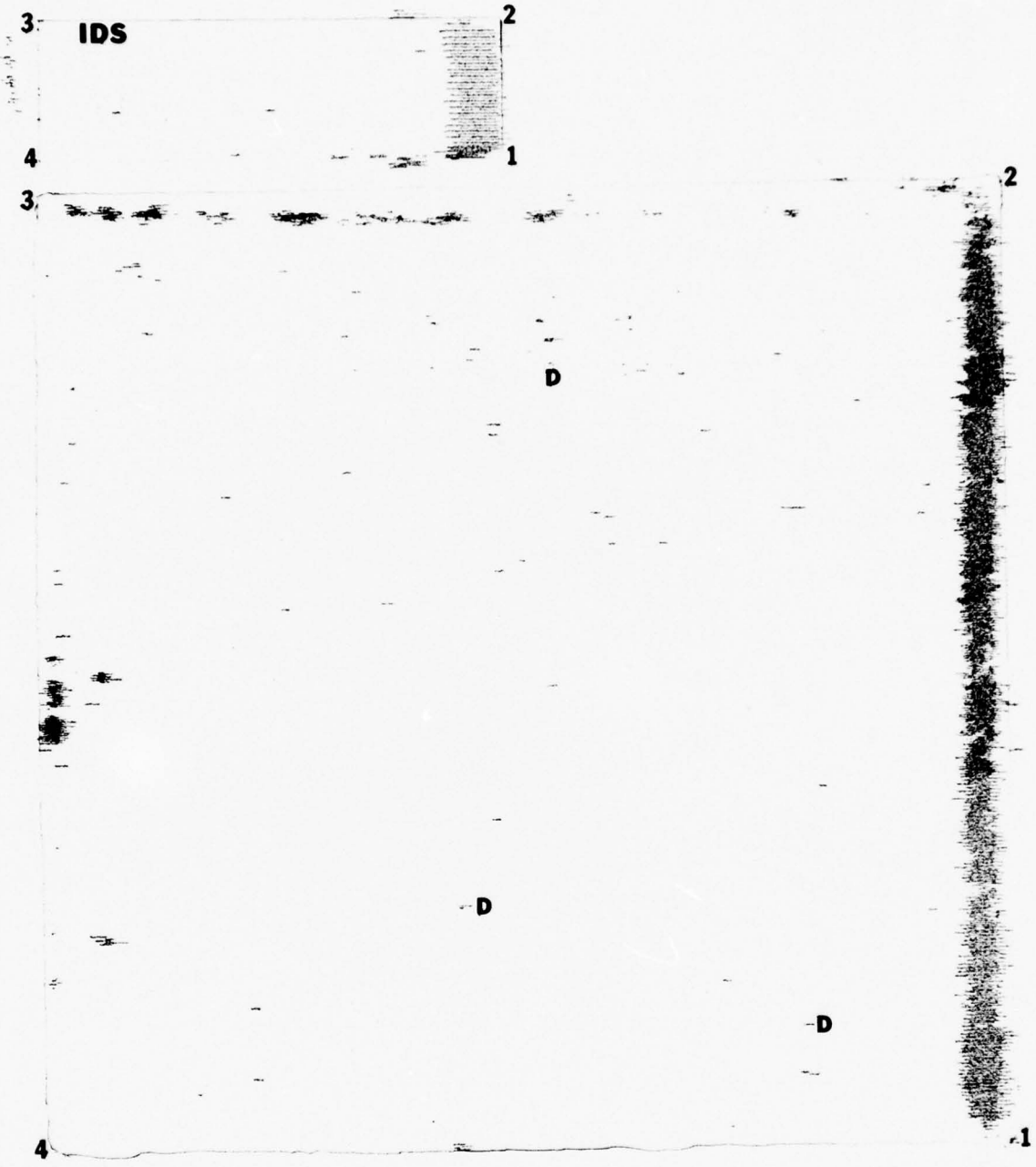


Figure 6. C-scan Recording of 45 MHz, 11° Ultrasonic Shear Wave Inspection of Ceralloy 147A Before Machining.


Figure 7. C-scan Recording of 45 MHz, 11° Ultrasonic Shear Wave Inspection of Ceralloy 147A after Machining.

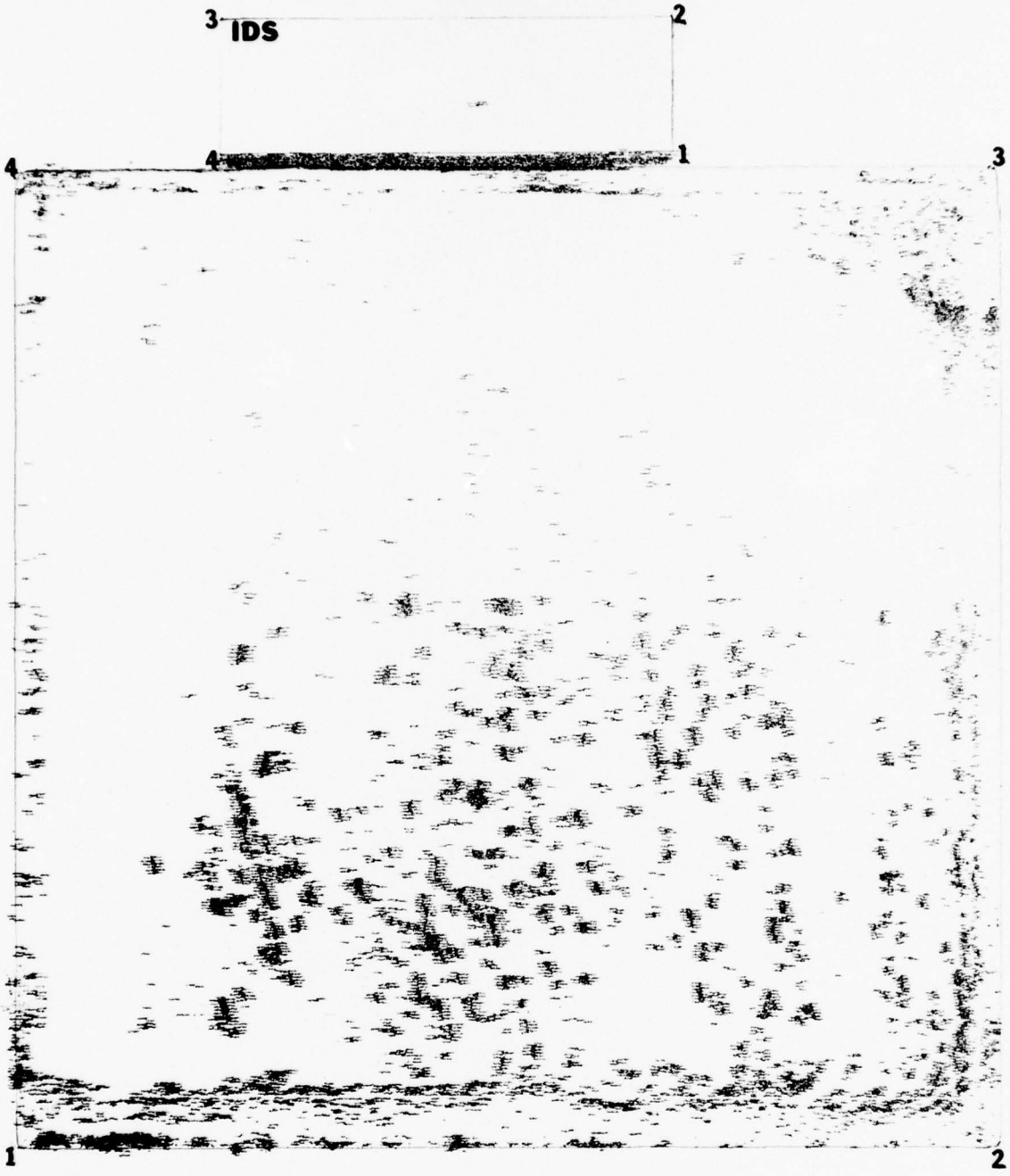


Figure 8. C-scan Recording of 45 MHz Longitudinal Wave Inspection of NC-132 Before Machining.

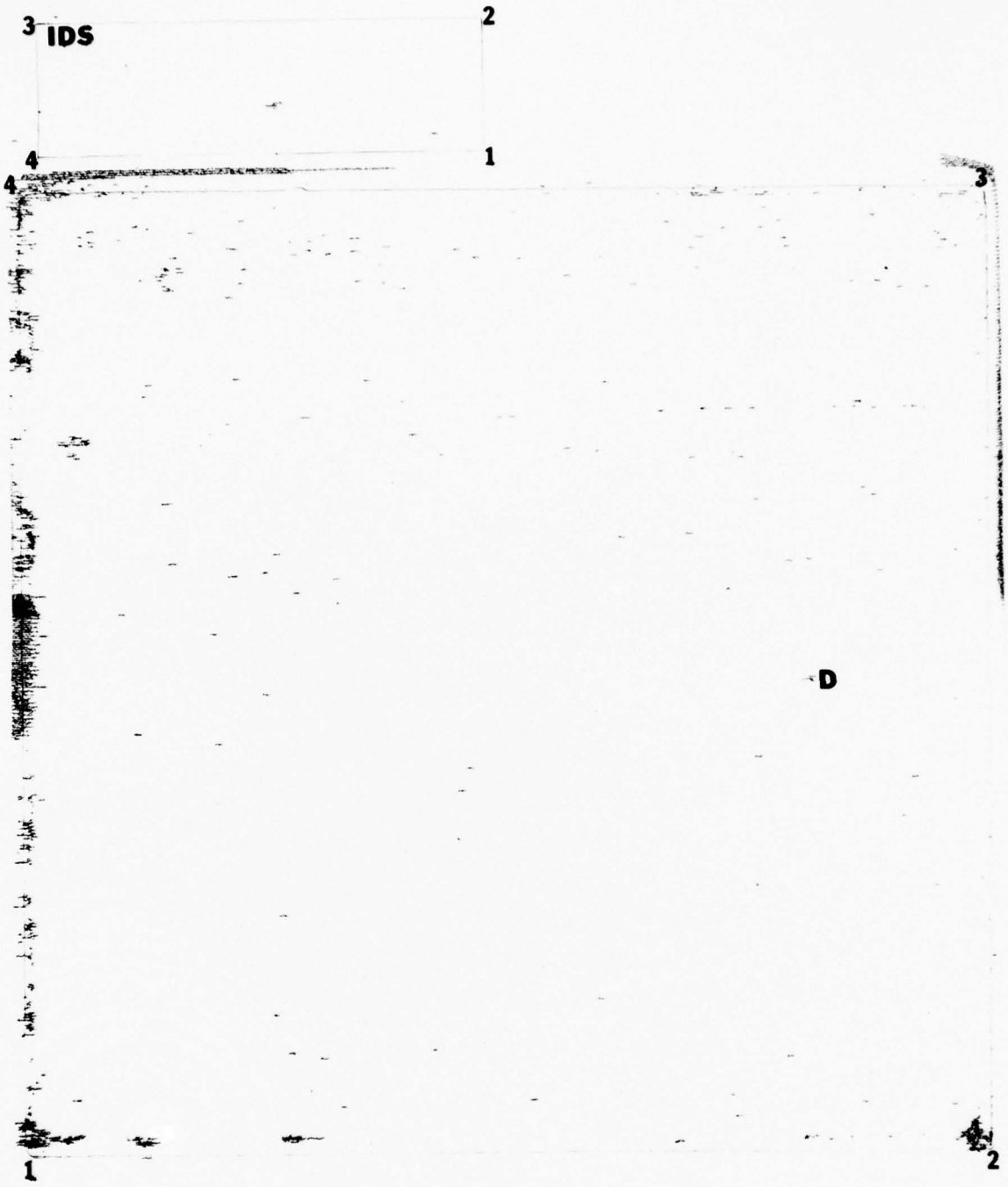


Figure 9. C-scan Recording of 45 MHz Longitudinal Wave Inspection of NC-132 After Machining.

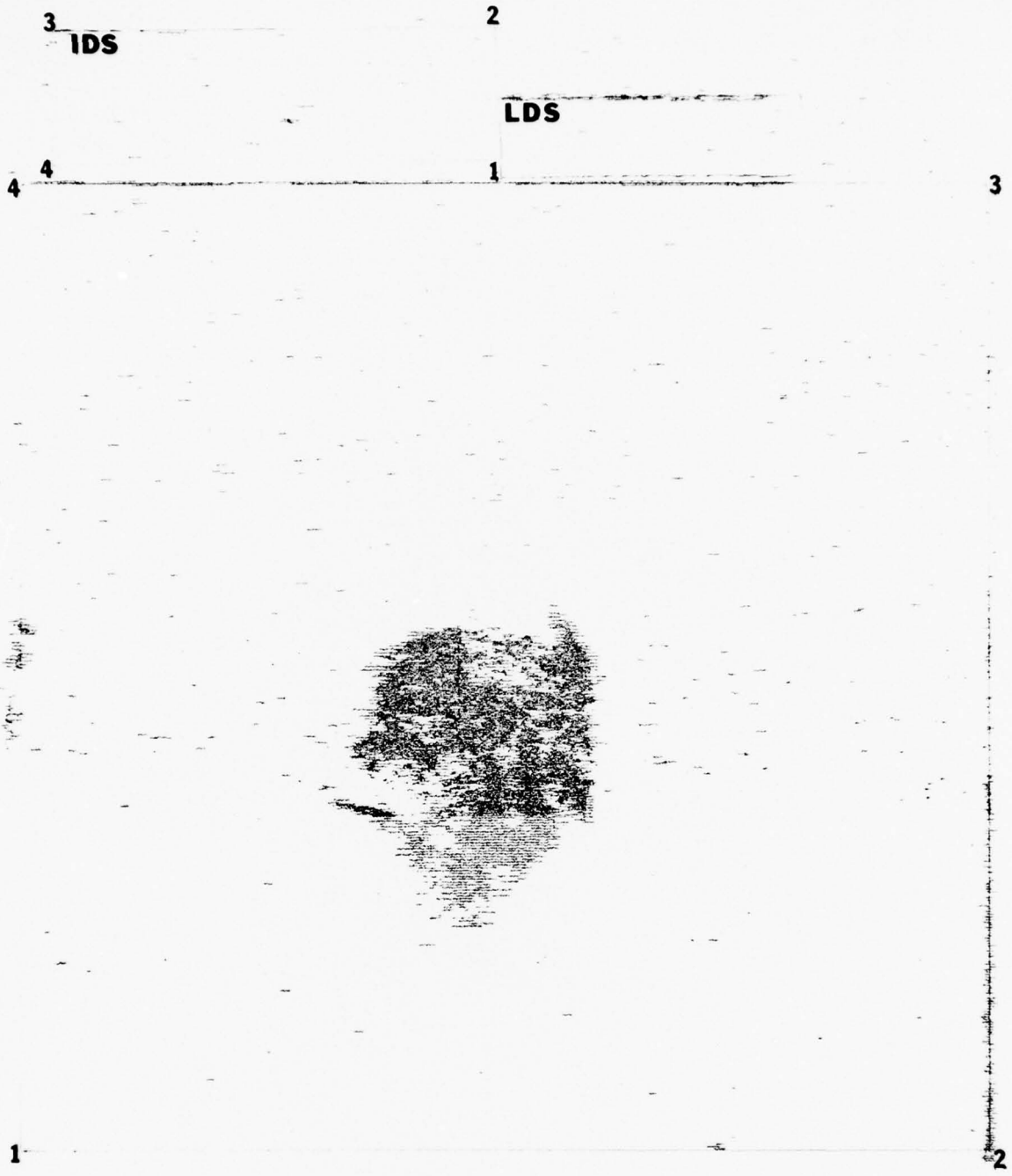


Figure 10. C-scan Recording of 45 MHz Longitudinal Wave Inspection of NC-203A Before Machining.

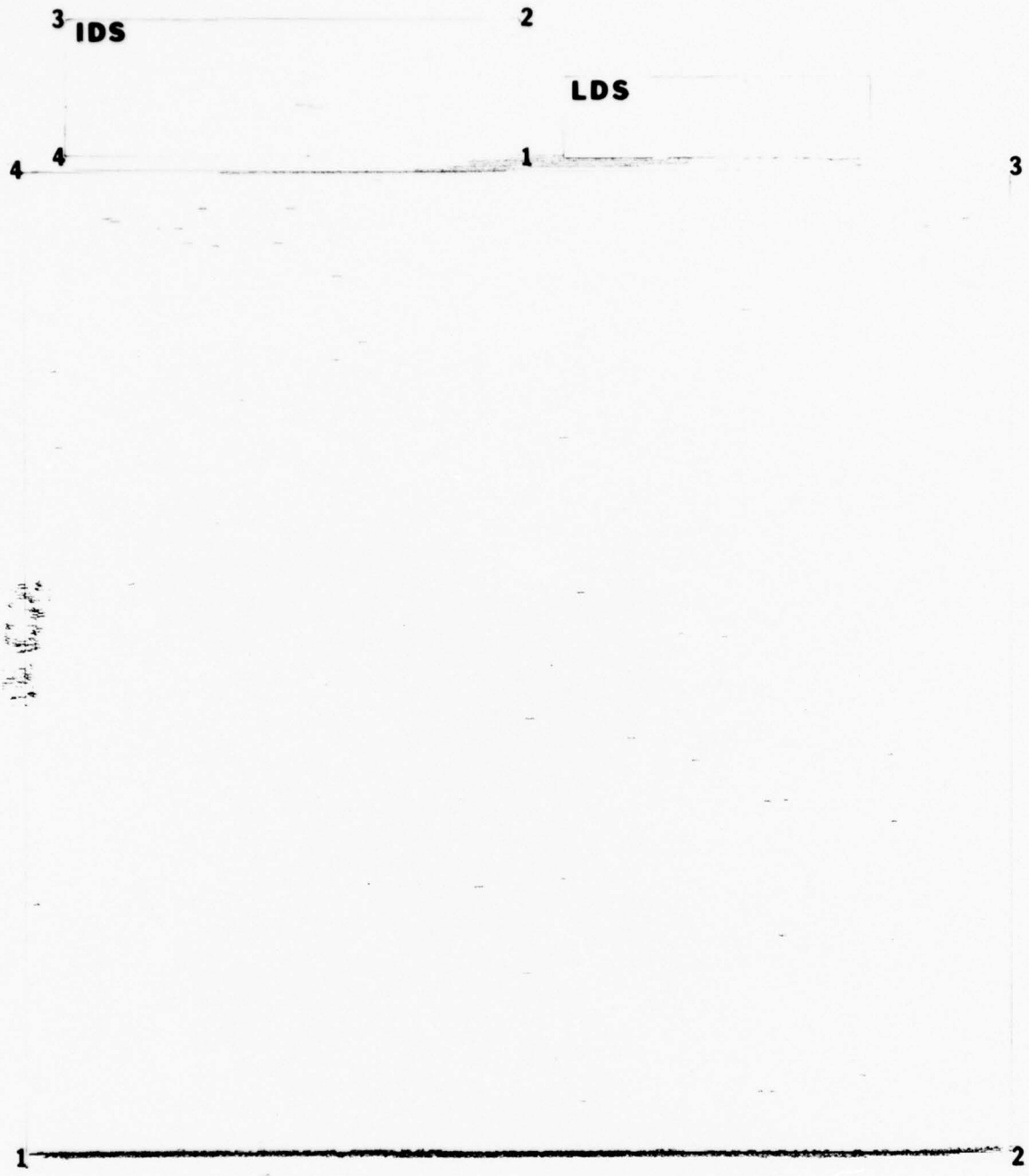


Figure 11. C-scan Recording of 45 MHz Longitudinal Wave Inspection of NC-203A After Machining.

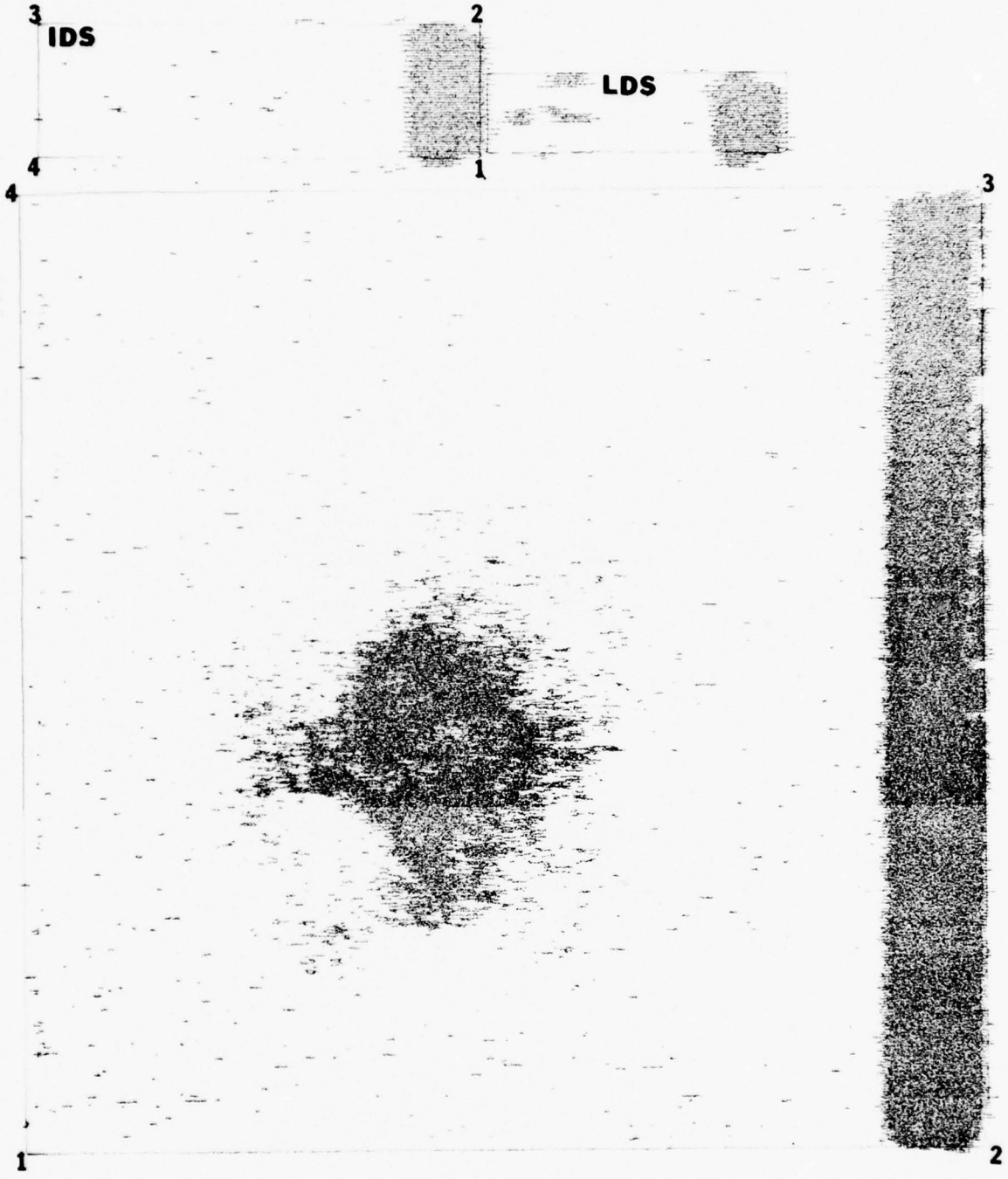


Figure 12. C-scan Recording of 45 MHz, 11° Shear Wave Inspection of NC-203A Before Machining.

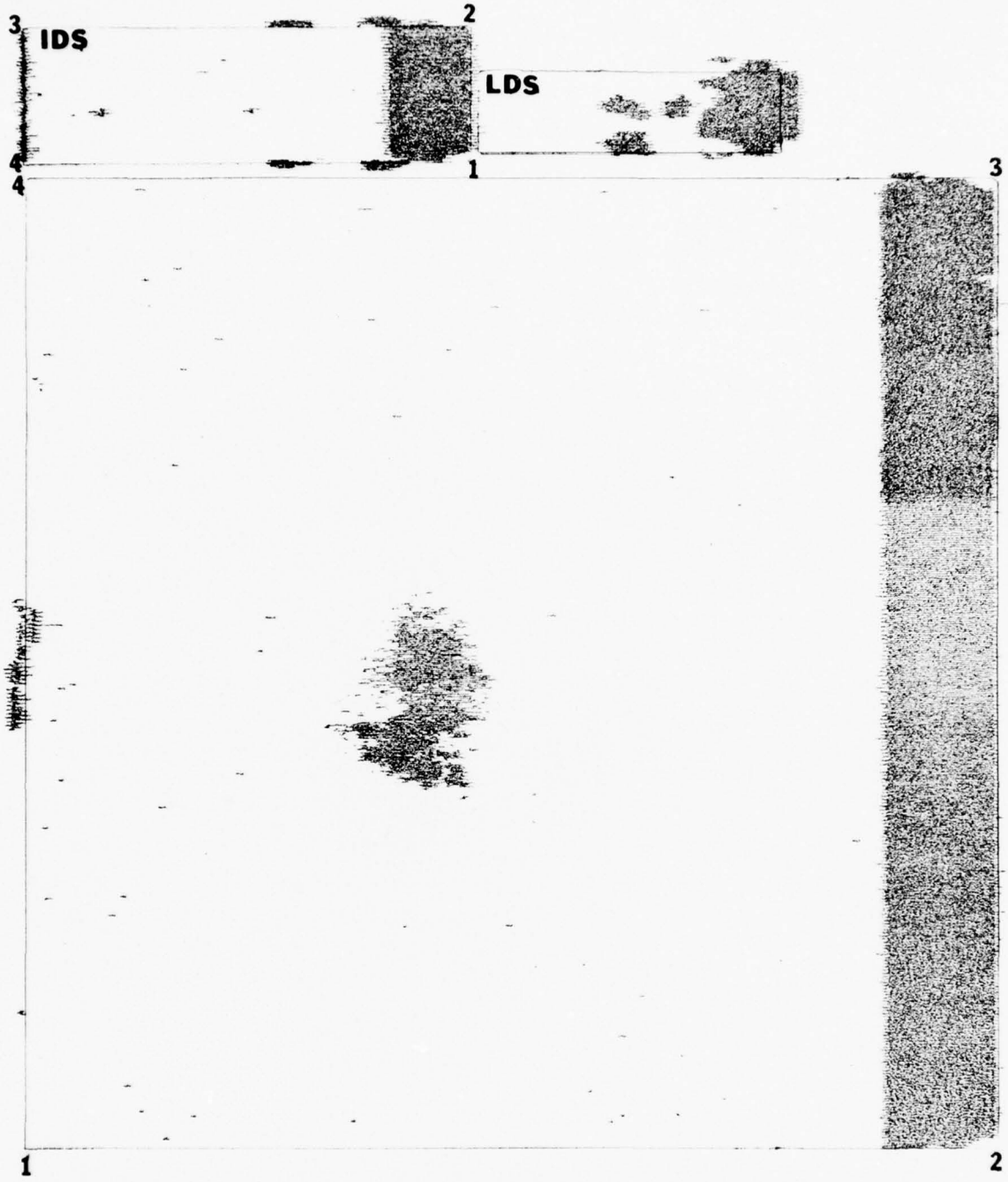


Figure 13. C-scan Recording of 45 MHz, 11° Shear Wave Inspection of NC-203A After Machining.

machining. After machining a smaller area remained on the bottom side as these scans were made. As can be seen in Figure 11, the longitudinal wave inspection with the beam focused at the center of the billet did not detect the area of porosity on the bottom side. The shear wave inspection (Figure 13), however, did detect the porosity near the bottom surface.

It is concluded from these inspections that significant surface flaws cause indications on the C-scans, but they also can mask internal defects. How much this effect might be a problem on an actual part, such as an airfoil, will have to be further evaluated. Surface flaws, as large as the ones removed by machining these specimens, are likely to be more serious than the internal flaws they mask.

### 4.3.2 Effect of Gate Length on Shear Wave Results

Figure 7 shows the IDS, LDS and billet of Ceralloy 147A inspected using the single gate width shear wave technique. Figure 14 shows the same scan made with the double gate width technique. In Figure 14 the deadband along the right hand edge of each part is twice as large as in Figure 7, the holes in the LDS are seen, the indications from the seeded defects in the IDS are larger and there are many more indications in the Ceralloy 147A. It was concluded from these scans that the double gate width technique offers improved sensitivity and reduces the probability of failing to detect a large defect (such as the holes in the LDS) due to unfavorable orientation.

### 4.3.3 Comparison of Longitudinal and Shear Wave Results

The Ceralloy 146A, which was inspected in the previous program using longitudinal waves and found to have only a few small defects, was not found to have any additional defects by shear wave inspection. The billets of NC-203A were also found to be relatively free of defects, except for the area of visible surface porosity near the center. This area was detected both by shear wave inspection from either side (Figures 13 and 15) and by longitudinal wave inspection from the same side (Figure 16). The A-scan display observed during the inspection shown in Figure 16 revealed that this defective area is not confined to the surface but extends somewhat into the material.

The billet of NC-132 was also relatively free of defects. In addition to one small defect detected by longitudinal wave inspection (labelled D in Figure 9), a number of mostly small defects were detected by the shear wave technique (Figures 17 and 18). These two figures show C-scan recordings for shear wave inspections made at two orientations 90° apart. The indications labelled D appear in both figures. Subsequent measurements of defect depths revealed most of these indications to be the result of residual surface pits that were too deep to remove by surface machining. In contrast, the billet of Ceralloy 147A was found to have a large number of defects scattered throughout the part (Figure 14). Because of the large number of scans and the large number of defects in each scan, it is difficult to present an overall recording of the inspection results on this billet which would clearly distinguish the circumstances under which each defect is detected. However, Figures 19 and 20 summarize the

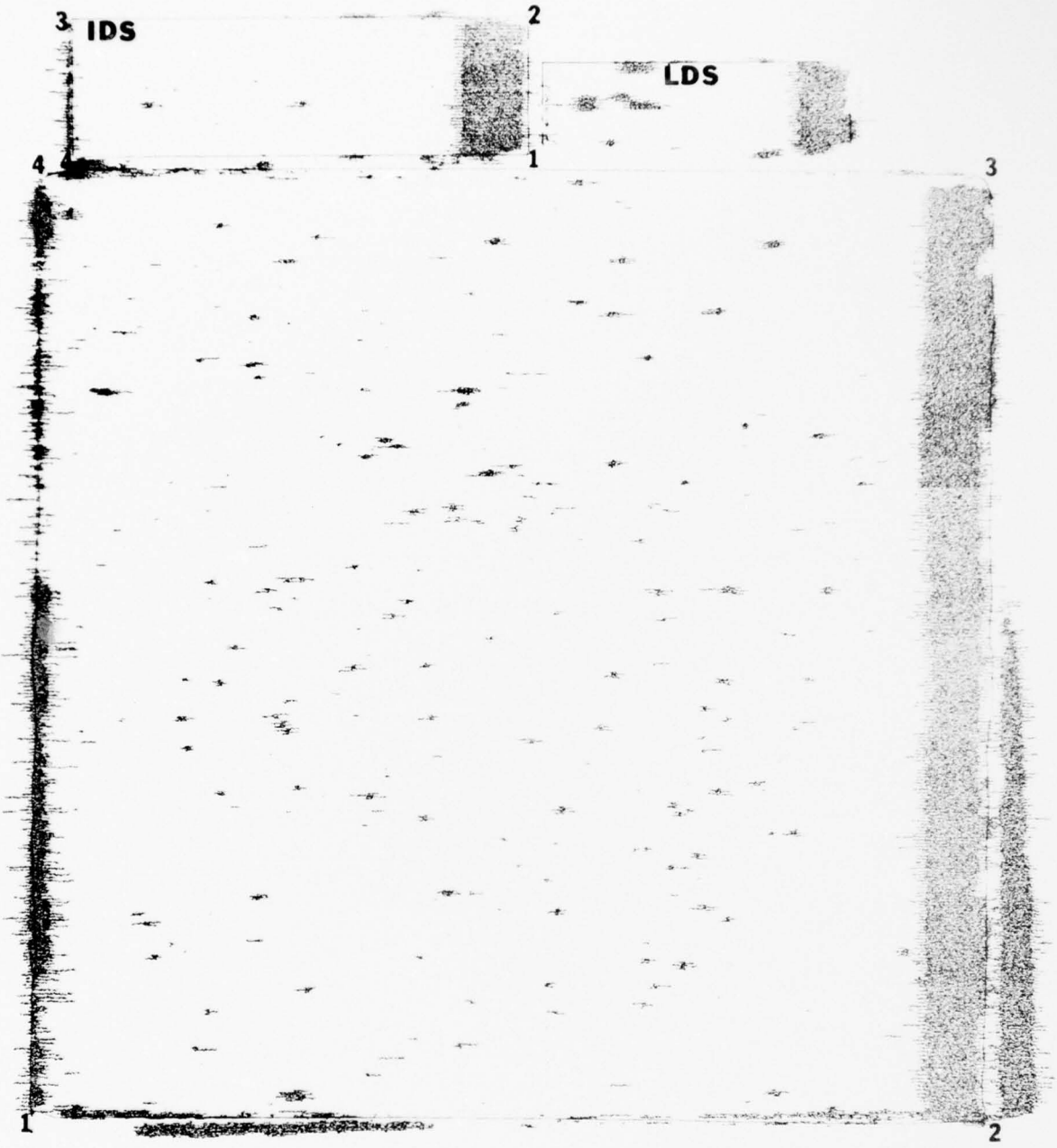


Figure 14. C-scan Recording of 45 MHz, 11° Shear Wave Inspection of Ceralloy 147A, After Machining Using Longer Defect Gate.

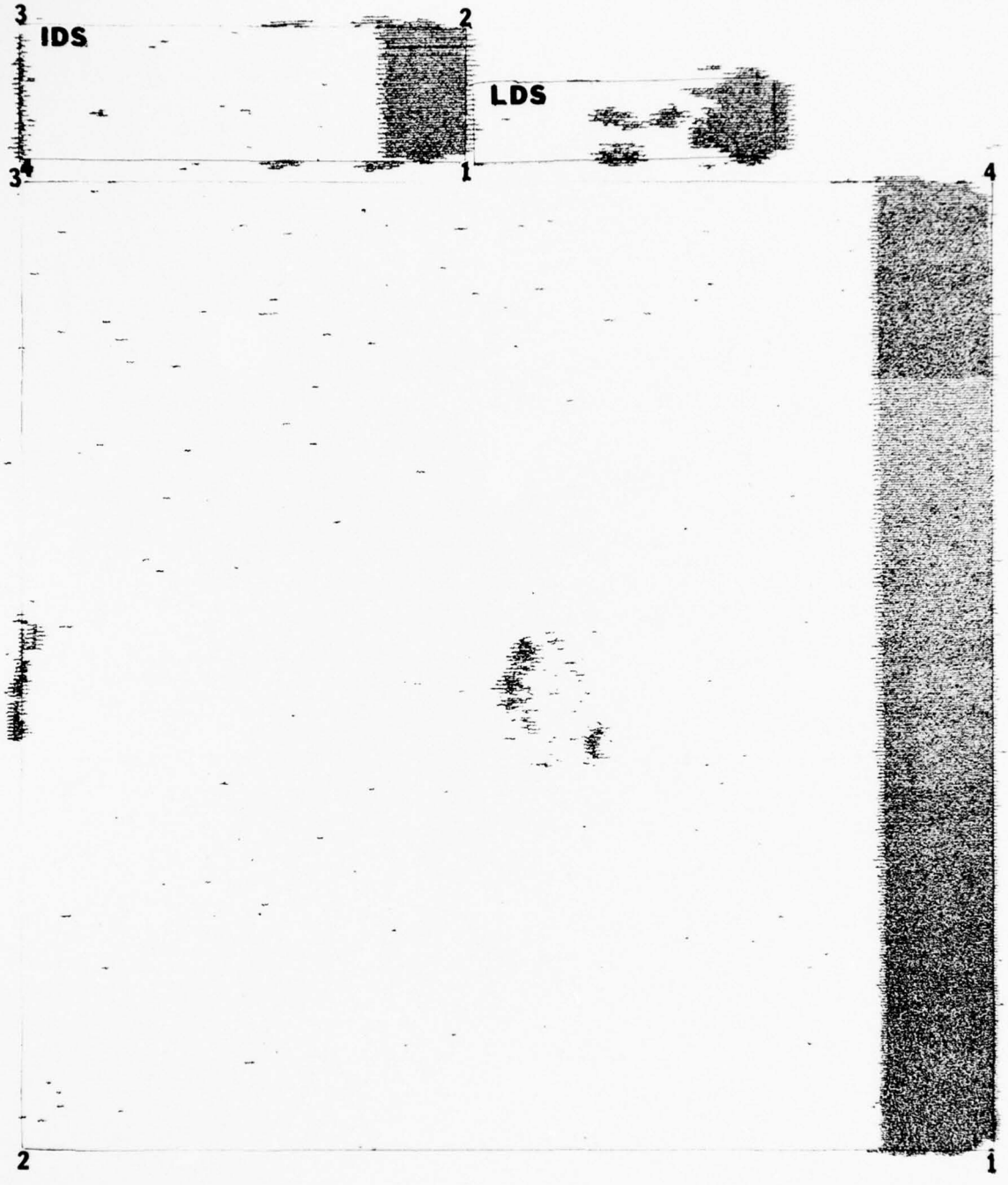


Figure 15. C-scan Recording of 45 MHz, 11° Shear Wave Inspection of NC-203A After Machining with Surface Porosity Up.

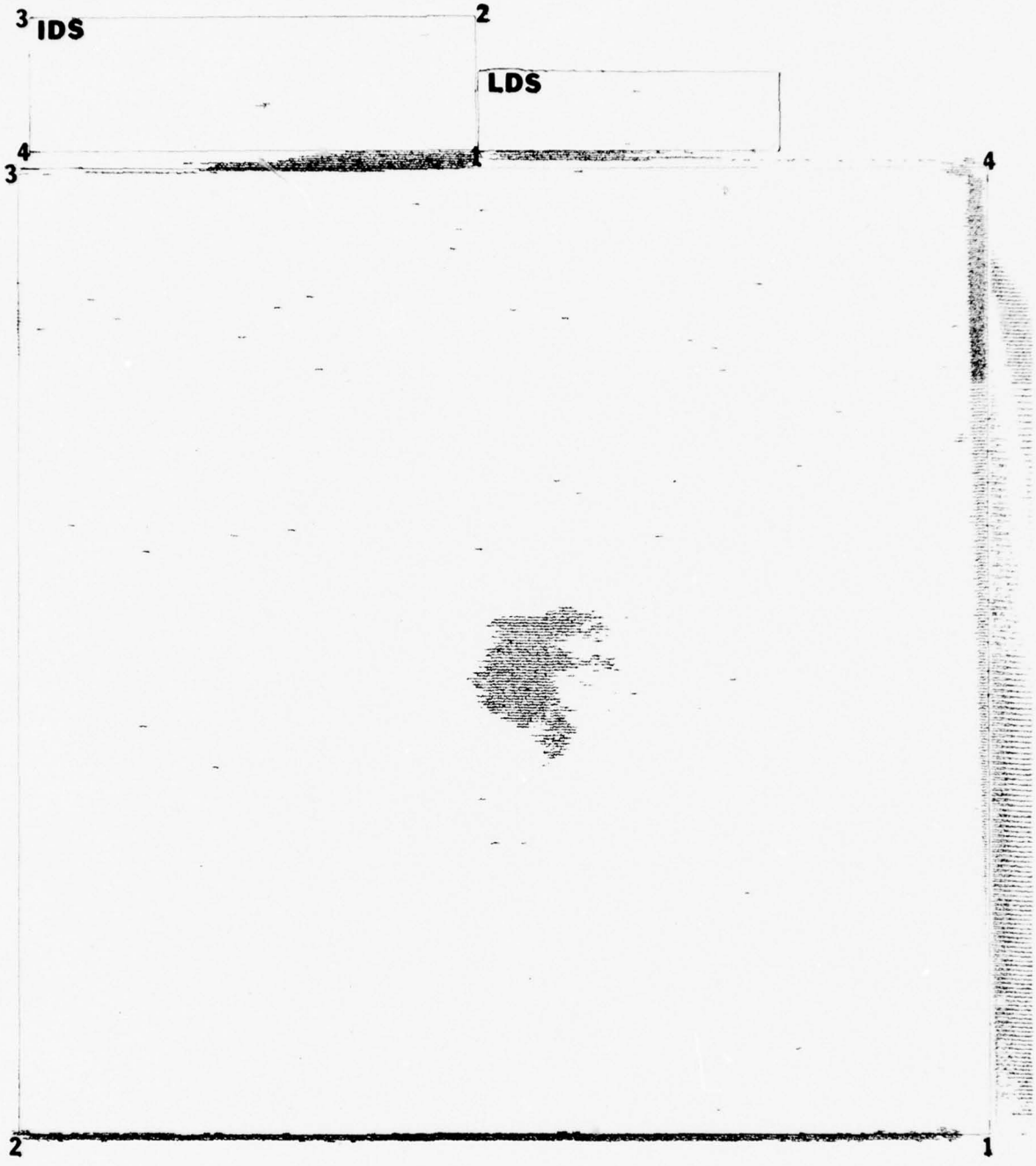


Figure 16. C-scan Recording of 45 MHz Longitudinal Wave Inspection of NC-203A After Machining with Surface Porosity Up.

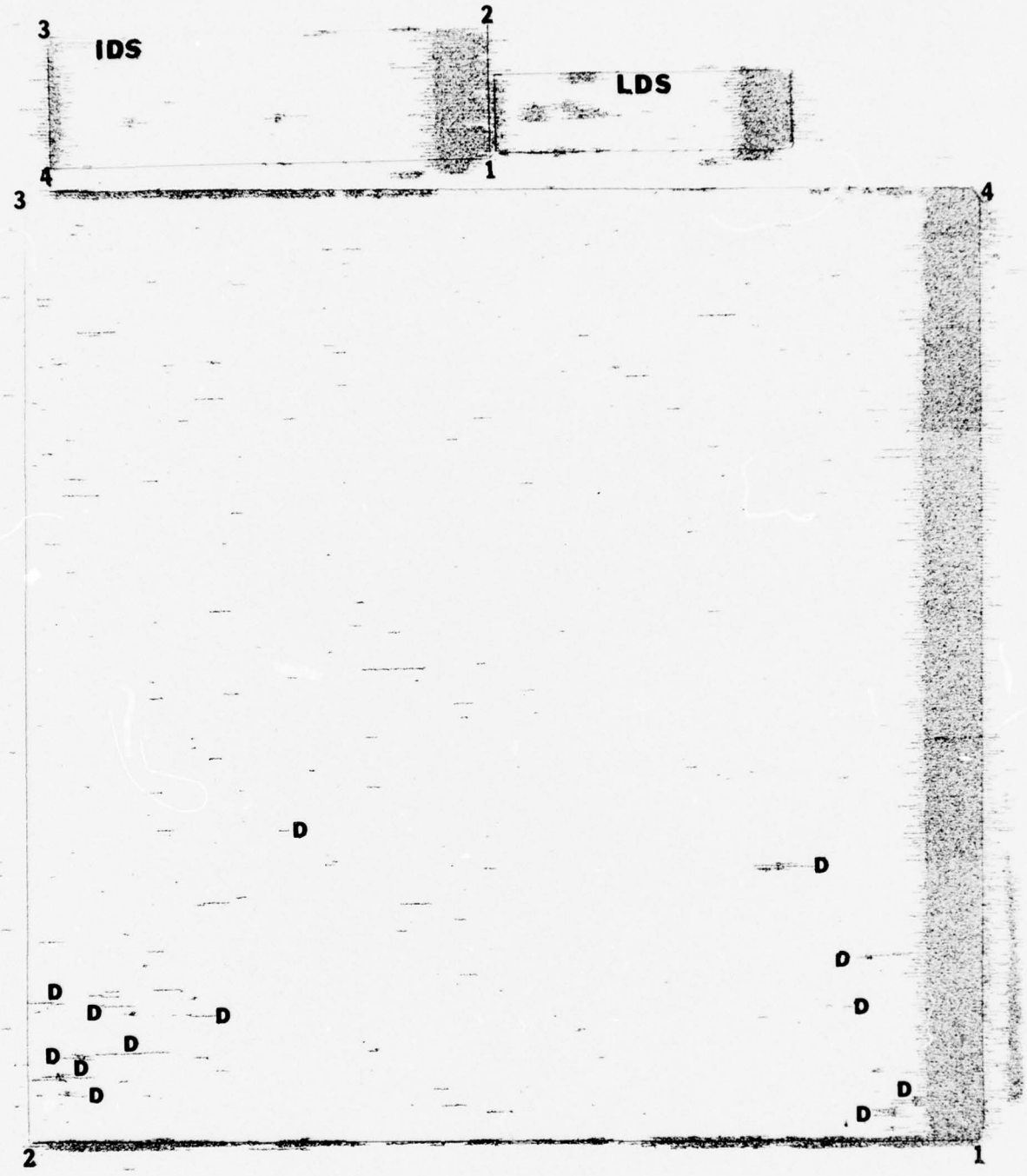


Figure 17. C-scan Recording of 45 MHz, 11° Shear Wave Inspection of NC-132.

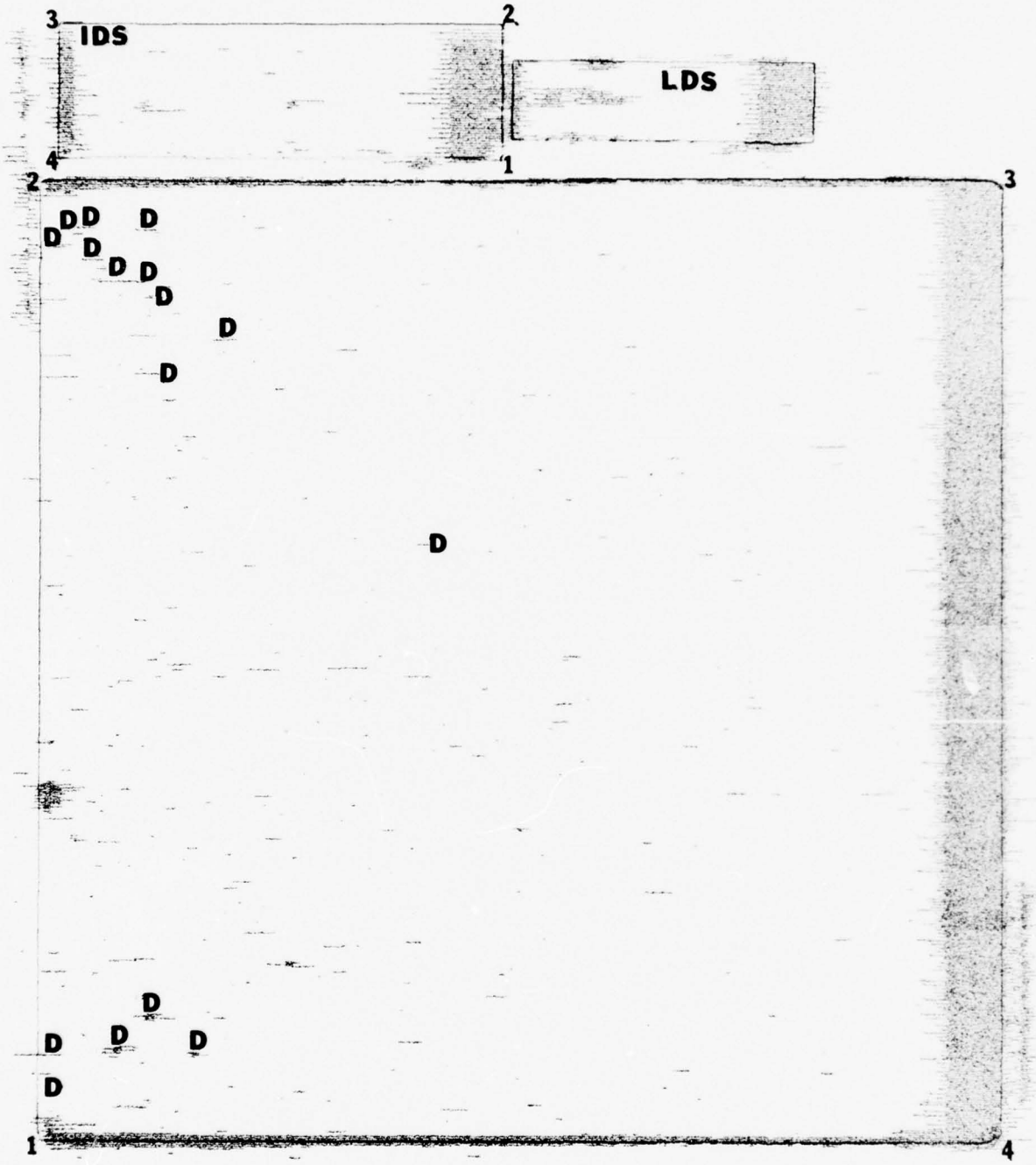


Figure 18. C-scan Recording of 45 MHz, 11° Shear Wave Inspection of NC-132 (Billet Rotated 90° from Figure 17).


Figure 19. Composite C-scan Recording of Three 45 MHZ Longitudinal Wave Inspections of the Billet of Ceralloy 147A.

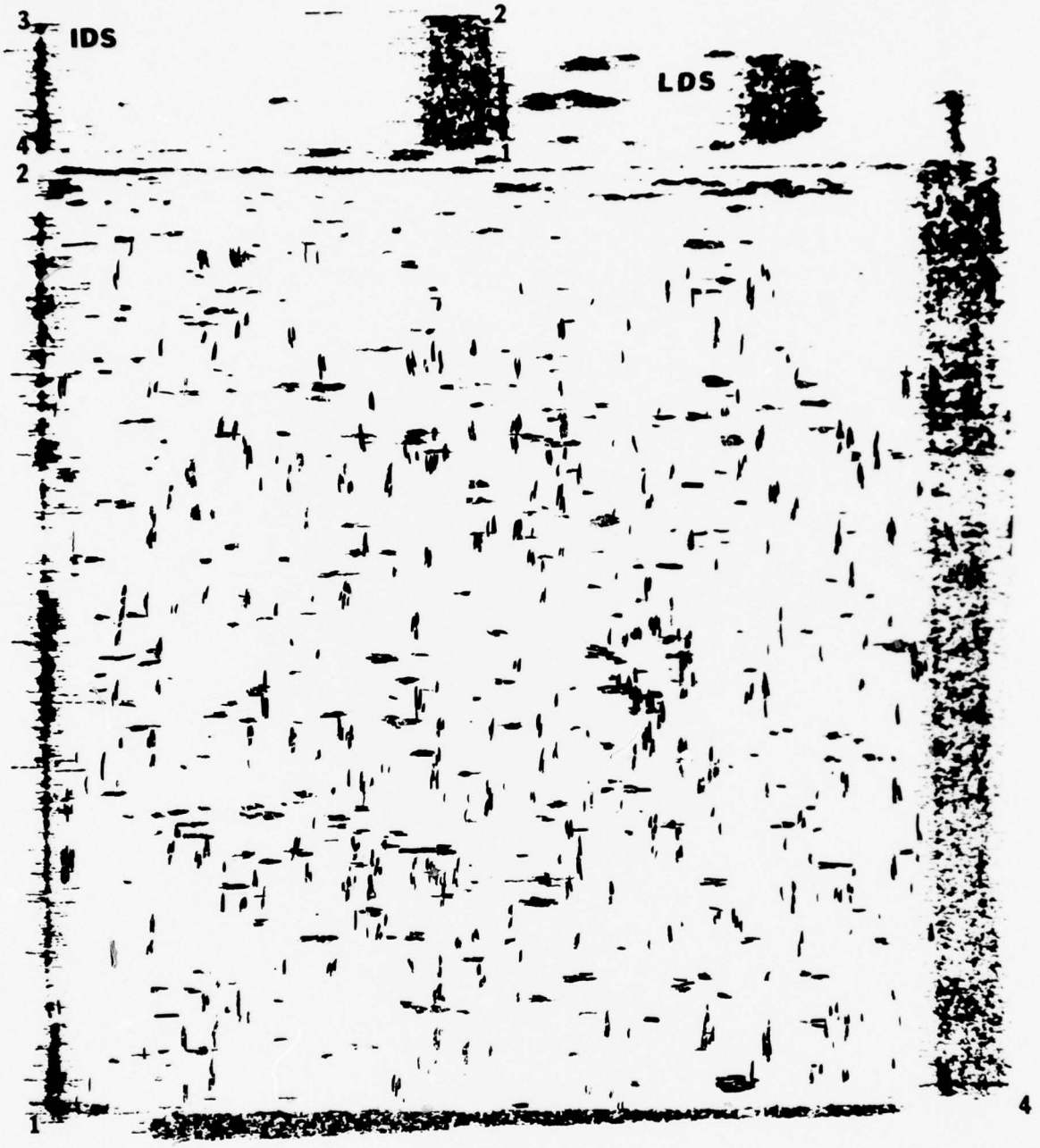


Figure 20. Composite C-scan Recording of Four 45 MHz, 11° Shear Wave Inspections of the Billet of Ceralloy 147A.

results of the longitudinal and shear wave inspections, respectively. Each figure was made by making a transparency from one C-scan recording and then laying that over the other C-scan recordings and tracing any new indications. Figure 19, therefore, is a composite of the three longitudinal wave inspections made at three different focal planes, while Figure 20 is a composite of the four shear wave inspections made at two orientations at each of two focal planes. In Figure 20 it should be noted that a number of cases exist where indications form a + or L shape. These are caused by defects that are detected from two different orientations 90° apart. The exact relationship between the two indications depends on the depth of the defect and on whether it was detected by the beam going down or up or both. By overlapping the two transparencies from which these figures were made the defects were identified that were only detected by shear wave inspection.

The following observations were made from a careful comparison of the various inspections of the billet of Ceralloy 147A:

1. The shear wave technique is capable of detecting substantially more defects than the longitudinal wave techniques, i.e., a large number of defects can only be detected by the shear wave technique;

2. A small number of defects were only detected by the longitudinal wave technique (it is natural to assume that these defects lie in an unfavorable plane to shear waves, i.e., in a plane parallel to the billet surfaces);

3. A large number of defects were only detected by one of the two inspections made 90° apart (showing the sensitivity of inspection beam orientation to defect orientation);

4. Some defects are only detected from one side of the billet (defects near a billet surface are outside of the focal plane of the transducer when that surface is up).

The results indicate that defect orientation has a significant effect, as expected, and that a number of scans are required to obtain complete part defect coverage.

The billet of sintered silicon carbide is quite small, so to obtain complete coverage four longitudinal wave inspections were performed, two 90° apart focused at the center and one focused near each surface from the opposite side. The C-scan recordings of these inspections are shown in Figures 21 to 24. One shear wave inspection was also performed on this billet. The C-scan recording (Figure 25) shows that the deadband covers almost half of this part. Because of this problem and because further evaluations of this billet in another program are planned, further shear wave inspections of this billet were not performed. The primary purpose of inspecting this billet was to determine the ability

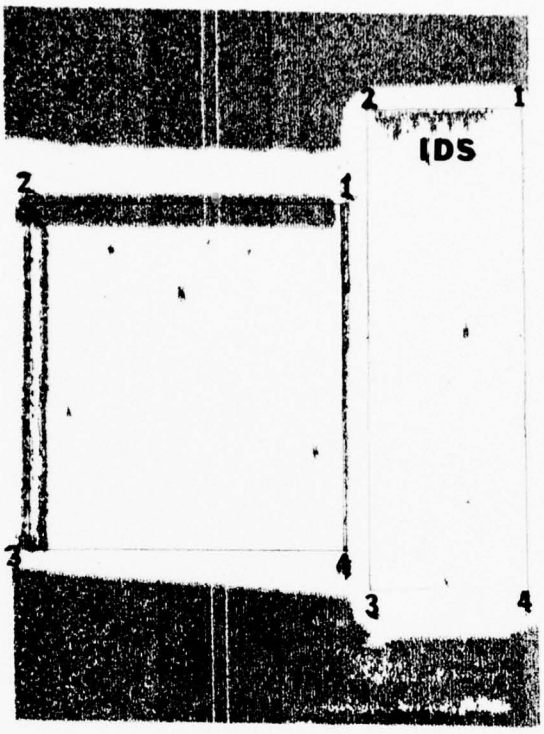


Figure 21. C-scan Recording of Ultrasonic Longitudinal Wave Inspection of Sintered Silicon Carbide Billet and Internal Defect Standard (IDS) at a Frequency of 45 MHz with a Water Path of 17 mm.

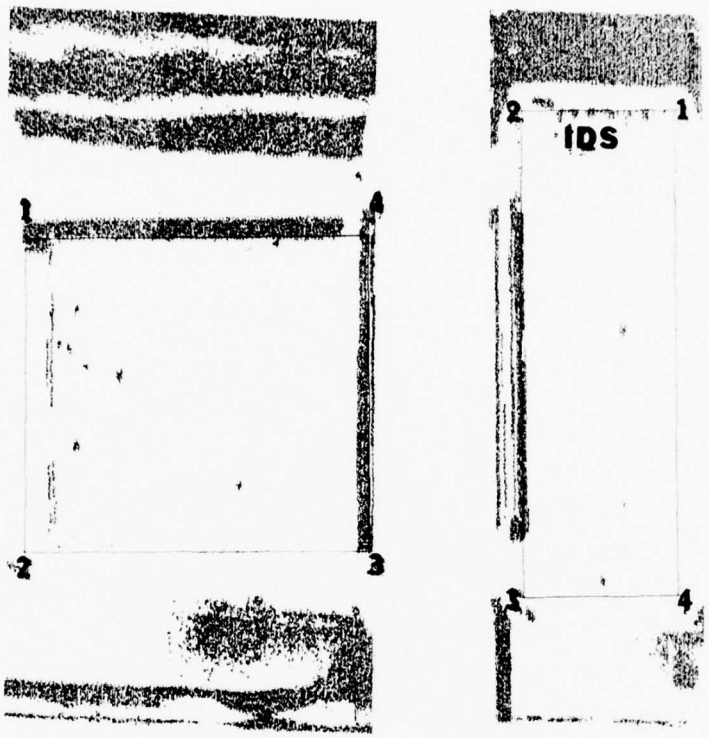


Figure 22. C-scan Recording of Ultrasonic Longitudinal Wave Inspection of Sintered Silicon Carbide Billet and Internal Defect Standard at a Frequency of 45 MHz with a Water Path of 17 mm.

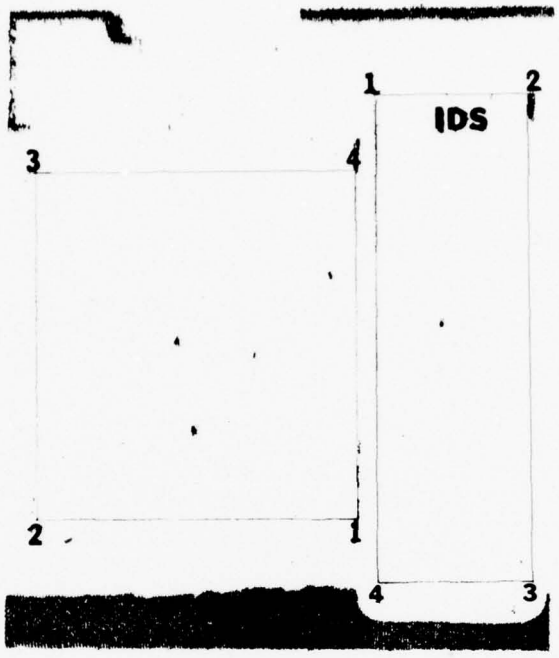


Figure 23. C-scan recording of Ultrasonic Longitudinal Wave Inspection of Sintered Silicon Carbide Billet and Internal Defect Standard at a Frequency of 5 mm (Top Side Down).

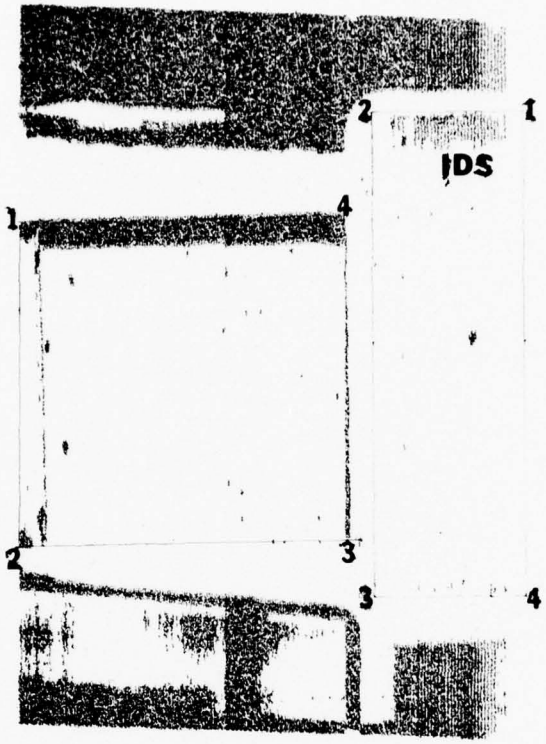


Figure 24. C-scan recording of Ultrasonic Longitudinal Wave Inspection of Sintered Silicon Carbide Billet and Internal Defect Standard at a Frequency of 45 MHz with a Water Path of 5 mm.

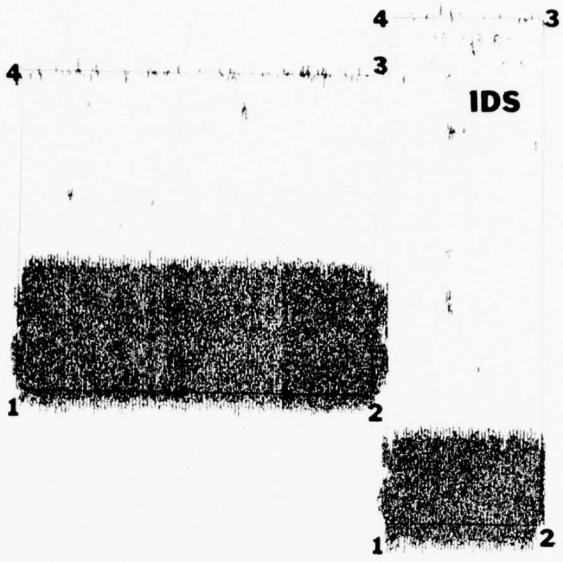


Figure 25. C-scan Recording of 45 MHz, 11° Shear Wave Inspection of Sintered Silicon Carbide Billet.

of high frequency ultrasonic inspection to detect the few small pores that are expected to be in this already well-characterized material. The four longitudinal scans revealed twenty-one different defects. The shear wave inspection showed five defects, three of which had not previously been detected, bringing that total to twenty-four. This is about double the number of pores the manufacturer expected to find in this sample. Further evaluations will be required to determine the reason for this unexpected result.

### 4.3.4 Measurement of Shear Wave Velocity and Defect Location

Based on the results of the ultrasonic inspections, twenty-five defects in the billet of Ceralloy 147A and six defects in the billet of NC-132 were selected for location measurement. Two criteria wereused to select these defects: 1) that they be detected by shear wave inspection only; and 2) that they be located so that a flexural strength specimen could be machined parallel to a billet edge to include the defect without interfering with another specimen on the edge of the billet. The techniques described in section 4.1 were used to measure the shear wave velocity and defect locations. The procedure was to make the defect measurements using two billet orientations 90° apart, in order to compare the measurements made using the shear beam (along the direction of beam travel) and by direct measurement of the transducer location (perpendicular to the direction of beam travel). At the same time that the defect location data was taken, shear velocity data was taken at five points along the edge of the billet. The data taken is summarized in Tables II and III along with calculated results. The measured value of the shear wave velocity for Ceralloy 147A is in excellent agreement with the calculated values in Table I, some of which were calculated using the longitudinal wave velocity in the same material. The shear wave velocity for NC-132 is significantly higher, indicating that the shear modulus is higher for this material. The calculated coordinates for defect locations are arranged to allow comparison of the two results. For the cases in Table II where two values are available the average errors were calculated to be 2.1 mm for X, 3.2 mm for Y and 0.48 mm for d. Since the specimen dimensions over which a uniform stress is applied are 6.4 x 19.1 mm, these accuracies were deemed adequate to place the detected defects within the uniform stress region. For the data in Table III the errors of 3.1 mm for X, 3.9 mm for Y and 0.21 mm for d if we ignore defect no. 4, where it appears two different defects were measured. In this case three of the four defects used for specimens were identified on the billet surface so that direct measurements could be made for machining specimens.

TABLE 11A

SHEAR WAVE VELOCITY RESULTS FOR CERALLOY 147A

| Parameters | Location Point Nos. | | | | | | | | | | Average and Std. Dev. |
|---|---|---|---|---|---|---|---|---|---|---|---|
| | X-Edge | | | | | Y-Edge | | | | | |
| | 1 | 2 | 3 | 4 | 5 | 6 | 7 | 8 | 9 | 10 | |
| T(μs) | 3.05 | 3.10 | 3.30 | 3.35 | 3.30 | 3.30 | 3.35 | 3.30 | 3.35 | 3.45 | 3.29±0.12 |
| c(mm) | 11.9 | 11.9 | 13.5 | 14.3 | 14.3 | 13.5 | 13.5 | 13.5 | 14.3 | 12.7 | 13.3±0.9 |
| t(mm) | 7.143 | 7.148 | 7.150 | 7.145 | 7.120 | 7.137 | 7.148 | 7.143 | 7.140 | 7.140 | 7.141±0.009 |
| φ(degrees)* | 39.37 | 39.77 | 43.35 | 45.02 | 45.12 | 43.40 | 43.36 | 43.38 | 45.04 | 41.65 | 42.99±2.00 |
| Vs(m/s)* | 6061 | 6098 | 5959 | 6035 | 6115 | 5953 | 5870 | 5956 | 6033 | 5539 | 5962±17 |
| Θ(degrees)* | 9.05 | 8.99 | 9.88 | 10.06 | 9.94 | 9.90 | 10.04 | 9.89 | 10.06 | 10.30 | 9.81±0.44 |

* Calculated Value

TABLE IIB

DEFECT LOCATION RESULTS IN CERALLOY 147A

| Defect No. | Direction of Shear Beam | | | | | | | | | | | | Specimen No. |
|---|---|---|---|---|---|---|---|---|---|---|---|---|---|
| | X | | | | | | Y | | | | | | |
| | c mm | T μs | Y mm | X(r)* mm | d* mm | Pulse cm | c mm | T μs | X mm | Y(r)* mm | d* mm | Pulse cm | |
| 1. | 142.1 | 1.85 | 34.9 | 134.6 | 6.22 | 3.4 | - | - | - | - | - | - | - |
| 2. | 84.9 | 2.40 | 11.1 | 75.2 | 3.82 | 1.8 | - | - | - | - | - | - | - |
| 2+. | 79.4 | 1.25 | 11.1 | 74.3 | 5.45 | 1.9 | - | - | - | - | - | - | - |
| 3. | 56.4 | 1.15 | 22.2 | 51.7 | 5.02 | 4.2 | 27.4 | 1.05 | 57.2 | 23.1 | 4.58 | 6.0 | 10 |
| 4. | 79.4 | 1.90 | 32.5 | 71.7 | 6.00 | 1.0 | 38.9 | 1.35 | 71.4 | 33.4 | 5.89 | 1.2 | 7 |
| 5. | 83.3 | 1.55 | 34.9 | 77.0 | 6.76 | 4.9 | - | - | - | - | - | - | - |
| 6. | 27.0 | 1.30 | 42.1 | 21.7 | 5.67 | 4.0 | 48.4 | 1.30 | 18.3 | 43.1 | 5.67 | 3.0 | 15 |
| 7. | 18.3 | 1.35 | 61.1 | 12.8 | 5.89 | 1.7 | 56.0 | 1.30 | 15.9 | 50.7 | 5.67 | 2.4 | - |
| 8. | - | - | - | - | - | - | 75.4 | 1.95 | 19.1 | 67.5 | 5.78 | 5.2 | - |
| 9. | 29.4 | 1.05 | 80.2 | 25.1 | 4.58 | 2.2 | 86.5 | 1.15 | 25.4 | 81.8 | 5.02 | 3.3 | 14 |
| 10. | 32.5 | 1.20 | 73.0 | 27.6 | 5.23 | 2.4 | 79.4 | 1.28 | 28.6 | 74.2 | 5.58 | 3.0 | - |
| 11. | 41.3 | 1.80 | 66.7 | 34.0 | 6.43 | 6.0 | 73.8 | 0.95 | 38.1 | 69.9 | 4.14 | 5.2 | 13 |
| 12. | 60.3 | 1.75 | 79.4 | 53.2 | 6.65 | 5.5 | 85.7 | 1.40 | 55.6 | 80.0 | 6.11 | 5.5 | 9 |
| 13. | - | - | - | - | - | - | 79.0 | 1.80 | 63.5 | 71.7 | 6.43 | 2.8 | - |
| 14. | 87.3 | 1.35 | 81.0 | 81.8 | 5.89 | 0.4 | 82.6 | 1.55 | 84.9 | 76.3 | 6.76 | 3.5 | 6 |
| 15. | 98.4 | 1.35 | 79.4 | 92.9 | 5.89 | 0.9 | 81.0 | 1.50 | 94.5 | 74.9 | 6.54 | 3.3 | - |
| 16. | 102.4 | 0.85 | 79.4 | 99.0 | 3.71 | 5.8 | 81.0 | 0.85 | 100.0 | 77.6 | 3.71 | 5.5 | 4 |
| 17. | 117.5 | 1.80 | 80.2 | 110.2 | 6.43 | 0.3 | 81.0 | 1.65 | 114.7 | 74.3 | 7.09 | 3.1 | - |
| 18. | - | - | - | - | - | - | 84.9 | 1.40 | 118.3 | 79.2 | 6.11 | 4.5 | 2 |
| 19. | 41.3 | 1.00 | 119.1 | 37.2 | 4.36 | 3.3 | 123.0 | 1.05 | 38.1 | 118.7 | 4.58 | 5.4 | 12 |
| 20. | 53.2 | 1.10 | 130.2 | 48.7 | 4.80 | 3.6 | 130.2 | 1.00 | 46.0 | 126.1 | 4.36 | 1.2 | 11 |
| 21. | - | - | - | - | - | - | 128.8 | 1.60 | 65.9 | 117.3 | 6.98 | 3.8 | 8 |
| 22. | 95.3 | 1.15 | 119.1 | 90.6 | 5.02 | 1.0 | - | - | - | - | - | - | 5 |
| 23. | 115.9 | 0.90 | 134.9 | 112.2 | 3.93 | 1.1 | 138.1 | 0.95 | 113.5 | 134.2 | 4.14 | 2.3 | 5 |
| 24. | 131.8 | 0.75 | 123.8 | 128.8 | 3.27 | 2.2 | 125.4 | 0.70 | 128.6 | 122.6 | 3.05 | 3.3 | - |
| 25. | 136.5 | 0.70 | 119.1 | 133.7 | 3.05 | 2.3 | 119.9 | 0.60 | 134.1 | 117.5 | 2.62 | 4.0 | 1 |

* Calculated value

\+ Defect measured both directly and after reflection of beam from bottom surface

TABLE IIIA

SHEAR WAVE VELOCITY RESULTS FOR NC-132

| Parameters | Location Point Numbers | | | | | | | | | | Average and Std. Dev. |
|---|---|---|---|---|---|---|---|---|---|---|---|
| | X-Edge | | | | | Y-Edge | | | | | |
| | 1 | 2 | 3 | 4 | 5 | 6 | 7 | 8 | 9 | 10 | |
| T(μs) | 2.95 | 2.95 | 2.90 | 2.85 | 2.85 | 2.70 | 2.65 | 2.70 | 2.80 | 2.80 | 2.82 ± 0.11 |
| c(mm) | 15.1 | 15.1 | 15.1 | 13.5 | 13.5 | 15.1 | 12.7 | 12.7 | 14.3 | 14.3 | 14.1 ± 1.0 |
| t(mm) | 5.845 | 5.839 | 5.842 | 5.837 | 5.837 | 5.837 | 5.842 | 5.839 | 5.842 | 5.839 | 5.840±0.003 |
| φ(degrees)* | 52.25 | 52.28 | 52.27 | 49.15 | 49.15 | 52.29 | 47.39 | 47.39 | 50.75 | 50.76 | 50.37±1.99 |
| $V_s$(m/s)* | 6473 | 6471 | 6584 | 6262 | 6262 | 7069 | 6512 | 6512 | 6595 | 6594 | 6533±224 |
| θ(degrees)* | 10.52 | 10.53 | 10.53 | 10.41 | 10.41 | 9.63 | 9.73 | 9.73 | 10.11 | 10.12 | 10.15±0.35 |

* Calculated value

## TABLE IIIB

## DEFECT LOCATION RESULTS IN NC-132

| Defect No. | Direction of Shear Beam | | | | | | | | | | | | Specimen No. |
|---|---|---|---|---|---|---|---|---|---|---|---|---|---|
| | X | | | | | | Y | | | | | | |
| | c mm | T μs | Y mm | X(r)* mm | d* mm | Pulse cm | c mm | T μs | X mm | Y(r)* mm | d* mm | Pulse cm | |
| 1 | 35.7 | 1.35 | 115.9 | 28.8 | 5.55 | 4.0 | 120.7 | 1.50 | 28.6 | 113.2 | 5.34 | 4.2 | 21 |
| 2 | - | - | - | - | - | - | 142.9 | 1.40 | 19.8 | 135.9 | 5.77 | 3.8 | - |
| 3 | 30.2 | 1.40 | 142.9 | 23.1 | 5.75 | 0.6 | 145.3 | 1.40 | 29.4 | 138.3 | 5.77 | 0.8 | 22 |
| 4 | 55.6 | 1.40 | 147.6 | 48.5 | 5.75 | 0.5 | 147.6 | 1.50 | 64.3 | 140.1 | 5.34 | 0.2 | 23 |
| 5 | 147.6 | 1.50 | 147.4 | 140.0 | 5.52 | 0.7 | 151.6 | 1.55 | 137.3 | 143.9 | 5.13 | 0.5 | 24 |
| 6 | 119.9 | 1.50 | 127.8 | 112.3 | 5.52 | 0.4 | - | - | - | - | - | - | - |

* Calculated Value

# 5.0 VERIFICATION OF ULTRASONIC EVALUATION BY MECHANICAL TESTING

The purpose of the mechanical testing was to expose the defects detected only by shear wave inspection for SEM fractography and to determine what correlation exists between defect indications and flexural strength. Standard four-point-bend testing was used with specimens machined so as to locate ultrasonically detected defects near the tensile surface. Since only the Ceralloy 147A contained a large enough number of defects to allow a significant number of defect-containing specimens to be machined, the majority of testing was done with this material. A few specimens of NC-132 containing surface defects were also tested.

## 5.1 Test Procedures

Standard bend tests were performed at room temperature using a tensile loading bend test jig with universal-joint coupling to ensure load alignment. Specimens with a two-to-one width-to-thickness ratio were tested at a constant crosshead speed of 0.51 mm/min(0.02 inches/min) with load pins having an inner span of 6.4 mm(1/4 inch) and an outer span of 19.1 mm (3/4 inch) to provide a "third point" load span. Moment and stress distributions during testing are shown schematically in Figures 26 and 27 with relevant dimensions and formulae. In Figure 27 the simple tensile stress, at some location Y above the neutral axis and between the inner loading pins, is indicated. If Y represents the location of a particular defect, and if a suitable stress concentration factor can be assigned to this defect, then a simple calculation would provide an estimate of the effective stress at this point from which it should be possible to predict the fracture strength of the specimen. Conversely, knowing the location of the defect and the fracture stress, a value for the stress intensity factor can be calculated.

## 5.2 Ceralloy 147A Hot Pressed Silicon Nitride

### 5.2.1 Specimen Preparation

Fifteen of the twenty-five defects whose locations were measured were selected for flexural strength specimens. The defects were selected to allow all of the specimens to be oriented in the same direction on the billet with no overlap and, to the extent possible, with the major axis of the defects perpendicular to the length of the specimen. The precision of the defect location data was also considered in selecting the defects. Figure 28 shows the specimens mapped out on the composite shear wave C-scan recording. The specimens were initially cut to the desired length (31.8mm) and width (6.4mm), but with the billet thickness. The bottom surface, as seen during defect location measurement, was machined to within 0.25 mm of the deepest measured defect location, and then the top surface was machined to obtain the final specimen thickness of 3.2mm. All of the long sides of each specimen were finish machined parallel to the specimen length with a 320 grit diamond wheel. The corners were then chamfered 0.1 mm at 45°.

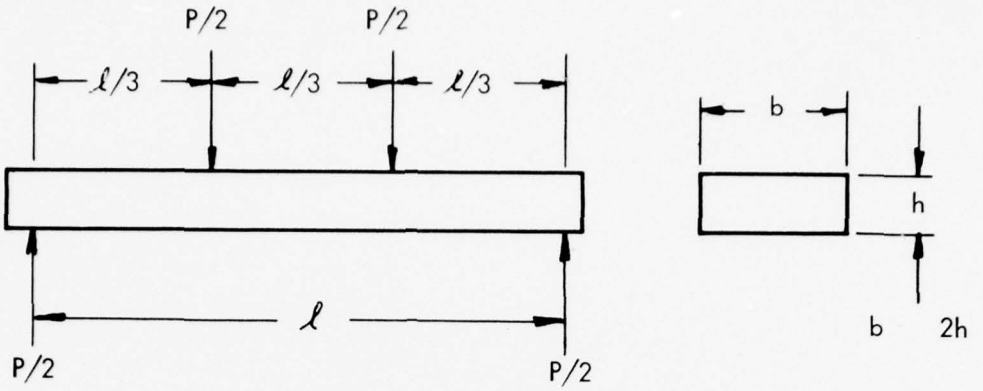


THIRD-POINT LOADING BEND TEST

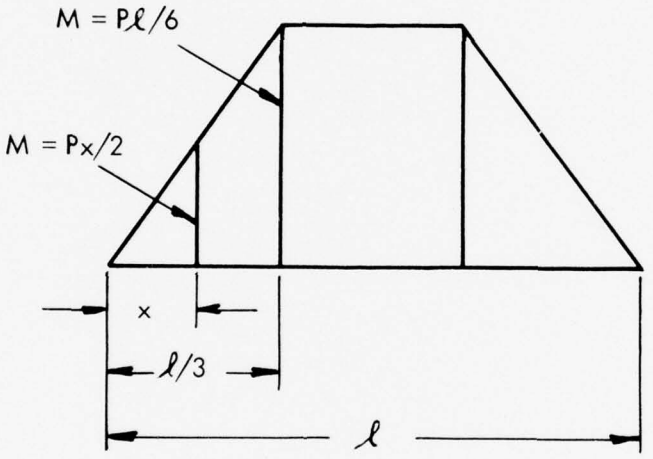


MOMENT DISTRIBUTION

Figure 26. Test Conditions for Flexural Strength Determinations.

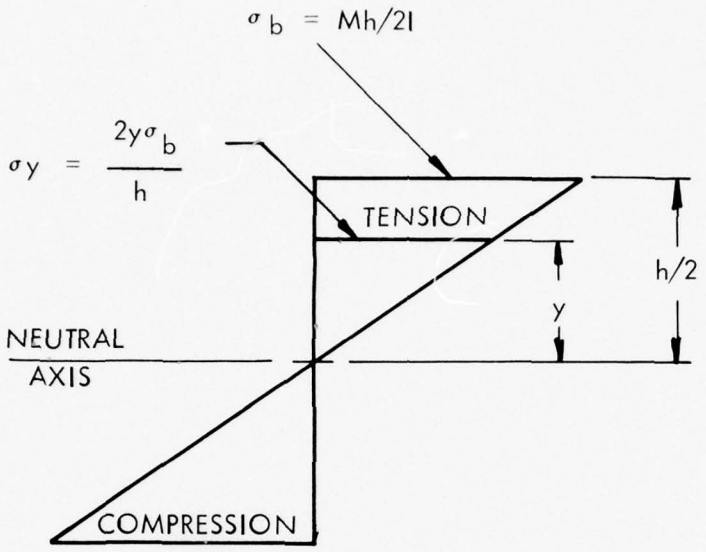


STRESS DISTRIBUTION

MOMENT OF INERTIA, I, ABOUT NEUTRAL AXIS (RECTANGULAR SECTION) = $\frac{bh^3}{12}$

$\sigma_b$ (OUTER FIBER) = $\frac{Mh}{2I} = \frac{P\ell}{6}\frac{h}{2I} = \frac{P\ell}{bh^2}$

$\sigma_y$ (FLAW) = K $\frac{2y\sigma_b}{h}$, WHERE K = GEOMETRIC STRESS CONCENTRATION FACTOR

Figure 27. Stress Distribution and Equations for Rectangular Bar Specimens.

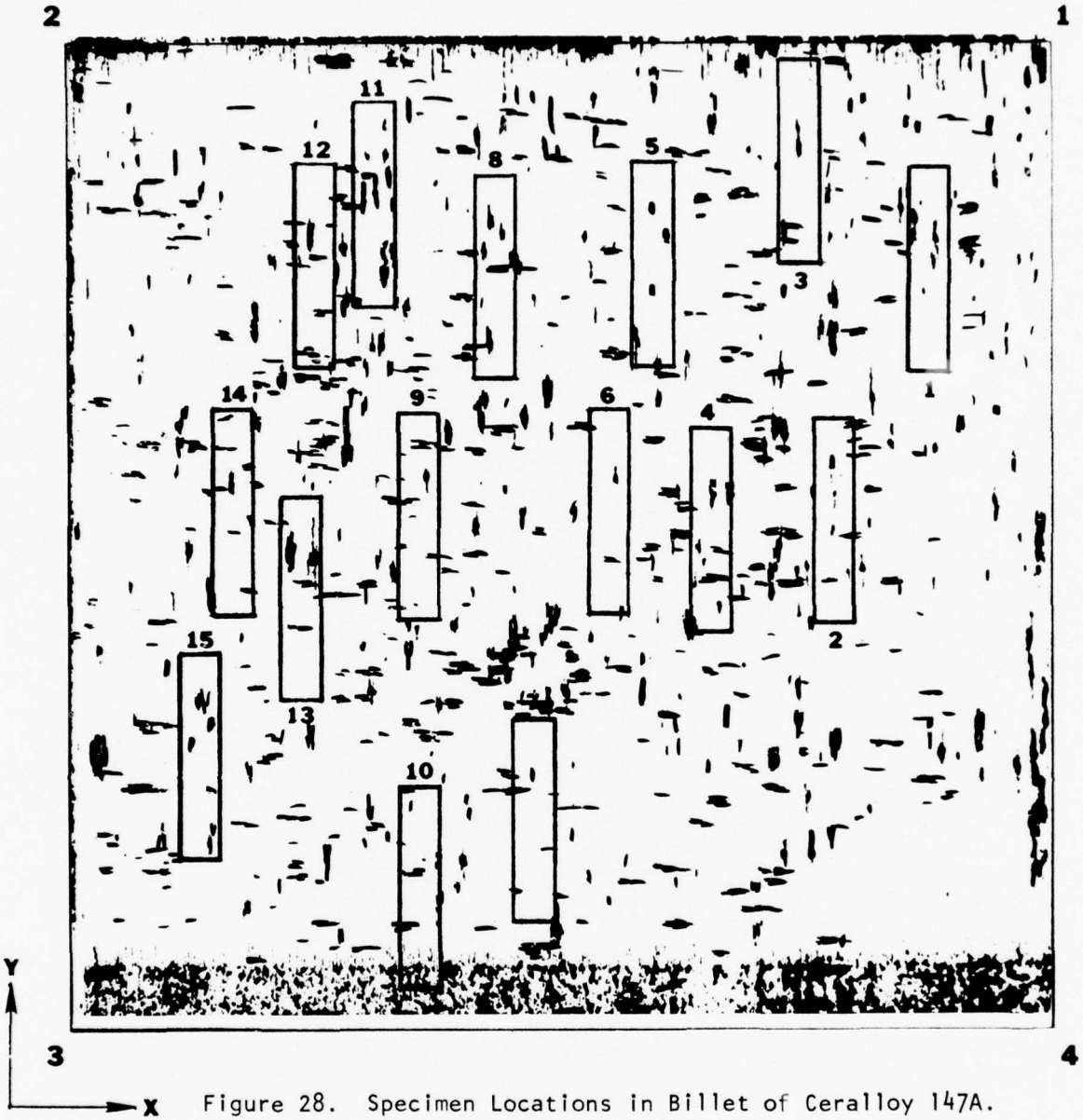


Figure 28. Specimen Locations in Billet of Ceralloy 147A.

### 5.2.2 Flexural Strength

Table IV lists the flexural strength of each specimen along with the distance of the fracture origin from the center and the pulse height of the ultrasonic signal from the defect. These pulse heights are given in cm and are referenced to a 5 cm signal from a 125 μm tungsten carbide seeded defect in the IDS. Since the transducer was not necessarily focused on the defect for these measurements, the pulse heights can not be expected to be an accurate indication of defect size. The average strength of these specimens is 609 $MN/m^2$. The strength of the strongest specimen, No. 12, is probably an anomaly since it was accidently machined 1.2 mm thinner than the others. The weakest specimens, Nos. 3, 8 and 9, fractured from apparent corner initiation sites. Of the remaining specimens, four have a high probability of having initiated failure at the ultrasonically detected defect. These specimens, Nos. 2, 6, 7 and 10, had an average strength of $605 \pm 91$ $MN/m^2$ ($87.6 \pm 13.2$ ksi). Of the other seven specimens, Nos. 4 and 13 appear to have broken through defects but this could not be confirmed because the fracture origin was lost due to specimen shattering. The other five, which broke at multiple surface origins had an average strength of $741 \pm 22$ $MN/m^2$ ($107.4 \pm 3.2$ ksi). Using the Student-t distribution these averages test significantly different at the 90% confidence level (Ref. 8).

### 5.2.3 SEM Fractography

Fracture surfaces of selected specimens were examined by scanning electron microscopy to identify and characterize any obvious fracture initiation sites. The primary purpose was to help identify those specimens that had broken through ultrasonically detected defects and to obtain an estimate of the size of these defects. A thin layer of vapor deposited copper ( 500Å) was applied to the surfaces to eliminate charging effects. In many of these specimens shattering occurred at the fracture surface, so that only one side of the fracture origin could be found.

Figure 29 shows the matching fracture surfaces of specimen #2 along with 200 and 1000X views of the fracture origin in the top low magnification view. The fracture origin is seen to be an area of about 100 by 40 μm of large crystals located approximately 300 μm below the tensile surface and 1.7 mm off center. This defect is similar to the large-grain, high density, silicon rich defects identified by Baumgartner and Richardson in HS 130 grade silicon nitride (Ref. 9). Figure 30 shows the fracture origin of specimen 6. At 50X the fracture origin, which is located about 1.6 mm off center in the specimen is seen as a V-shaped defect at the surface with a small semi-circular mirror region. At successively higher magnifications, this defect appears to be a crack running in perpendicularly from the specimen surface and then branching into an inverted Y. The fracture origin of specimen 7 is shown in Figure 31 at 50 and 200X. It is a small defect at the center of the specimen, 60μm below the tensile surface. Figure 32, which shows both sides of the defect at 1000X, indicates that one side of the specimen contains a hole which was left by material which pulled out and

TABLE IV

FLEXURAL STRENGTH OF HOT PRESSED $Si_3N_4$

1. Ceralloy 147A

| Specimen No. | Pulse Ht.cm | Flexyral Strength $MN/m^2$ | ksi | Fracture Location Along Length mm from center | HiX SEM |
|---|---|---|---|---|---|
| 1 | 4.0 | 717 | 104.0 | 2.4 | No |
| 2 | 4.5 | 683 | 99.1 | 1.9 | Yes |
| 3 | 2.3 | 191 | 27.7 | 3.6 | Yes |
| 4 | 5.5 | 645 | 93.6 | 4.0 | No |
| 5 | 1.0 | 728 | 105.6 | 2.4 | No |
| 6 | 3.5 | 619 | 89.8 | 1.5 | Yes |
| 7 | 1.2 | 636 | 92.3 | 1.3 | Yes |
| 8 | 3.8 | 388 | 56.3 | 5.1 | No |
| 9 | 5.5 | 330 | 47.9 | 0.8 | Yes |
| 10 | >6 | 472 | 68.5 | 0.0 | Yes |
| 11 | 1.2 | 733 | 106.3 | 3.6 | Yes |
| 12 | 5.4 | 793 | 115.1 | 0.8 | No |
| 13 | 5.2 | 669 | 97.1 | 1.8 | Yes |
| 14 | 3.3 | 754 | 109.4 | 0.4 | No |
| 15 | 3.0 | 771 | 111.8 | 2.4 | No |
| 2. NC-132 | | | | | |
| 21 | 4.2 | 367 | 53.2 | 0.0 | Yes |
| 22 | 0.8 | 322 | 46.7 | 0.5 | Yes |
| 23 | 0.2 | 369 | 53.5 | 1.5 | Yes |
| 24 | 0.5 | 456 | 66.2 | 2.4 | Yes |

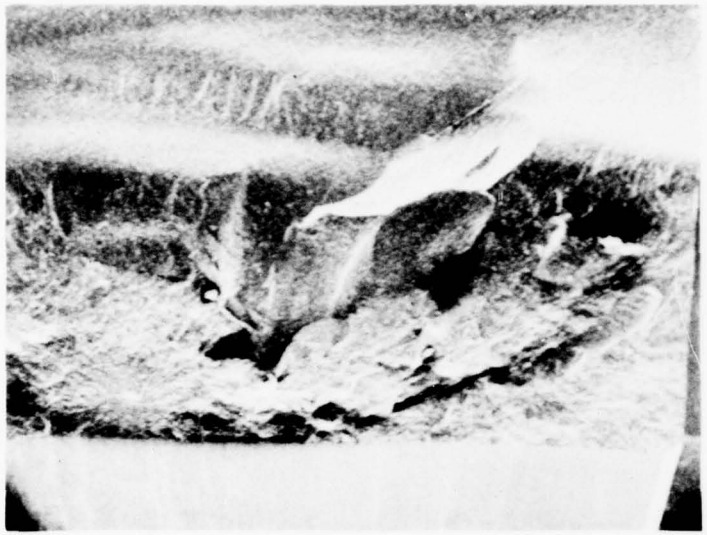

16X

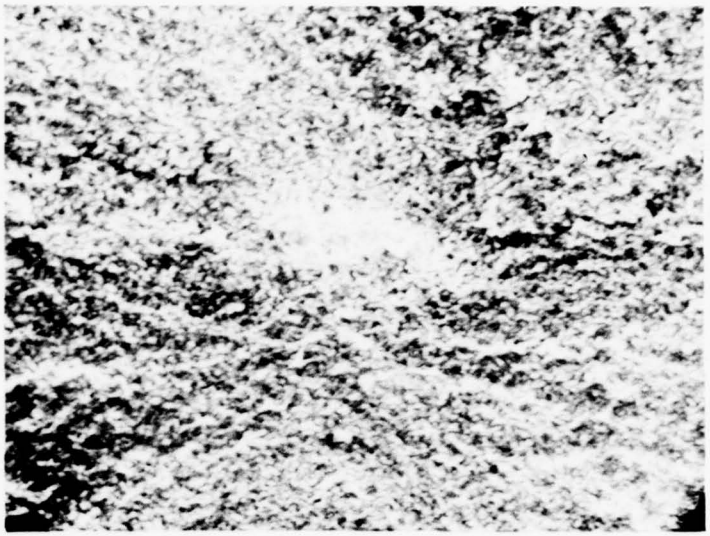

200X

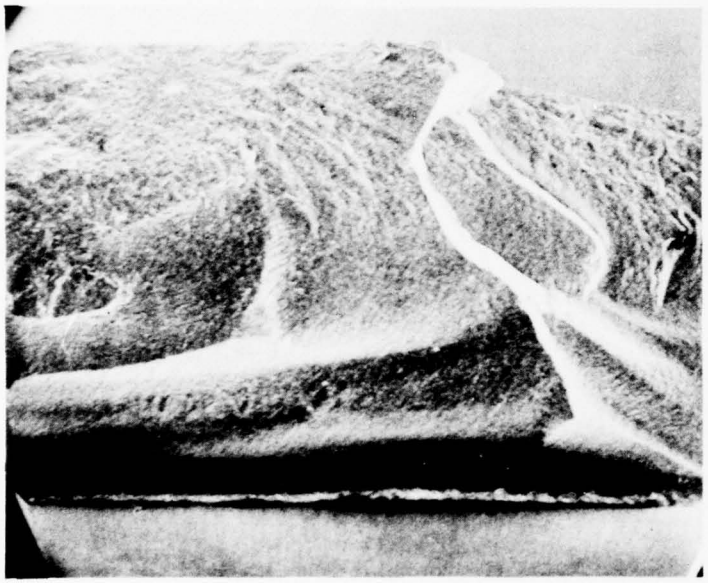

16X

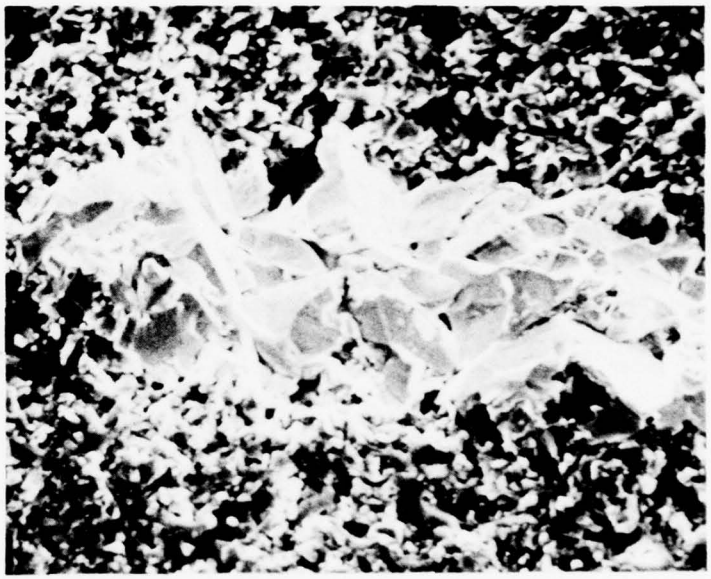

1000X

Figure 29. Fracture Surfaces of Ceralloy 147A Specimen 2 Showing Fracture Initiation Site.

50X

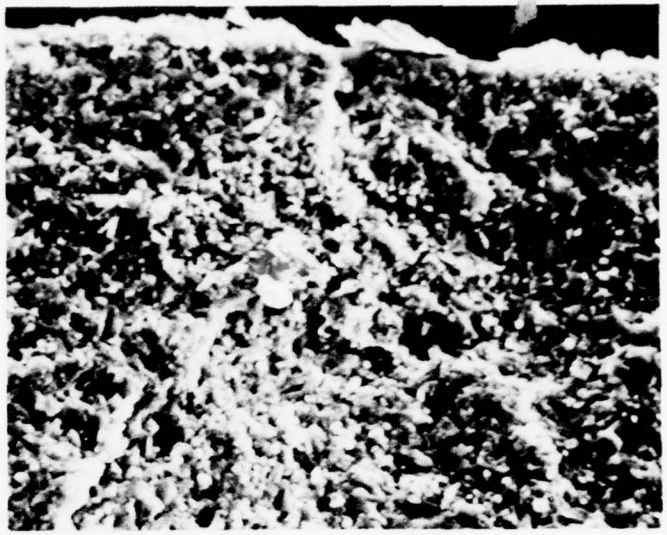

1000X

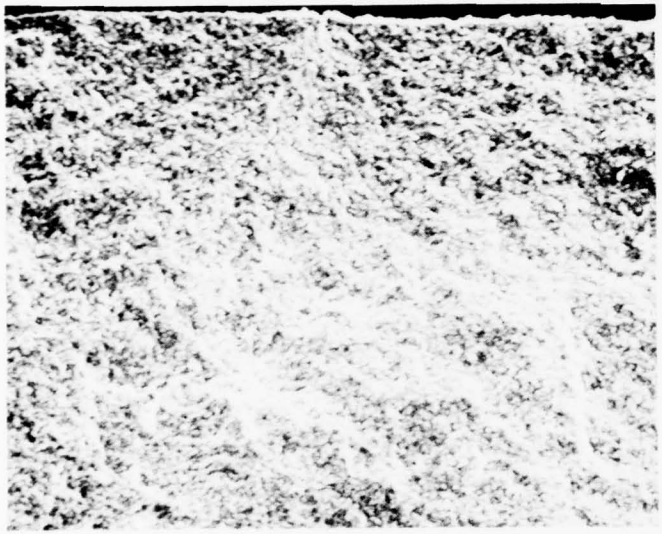

200X

2000X

Figure 30. Fracture Surface of Ceralloy 147A Specimen 6 Showing Fracture Initiation Site.

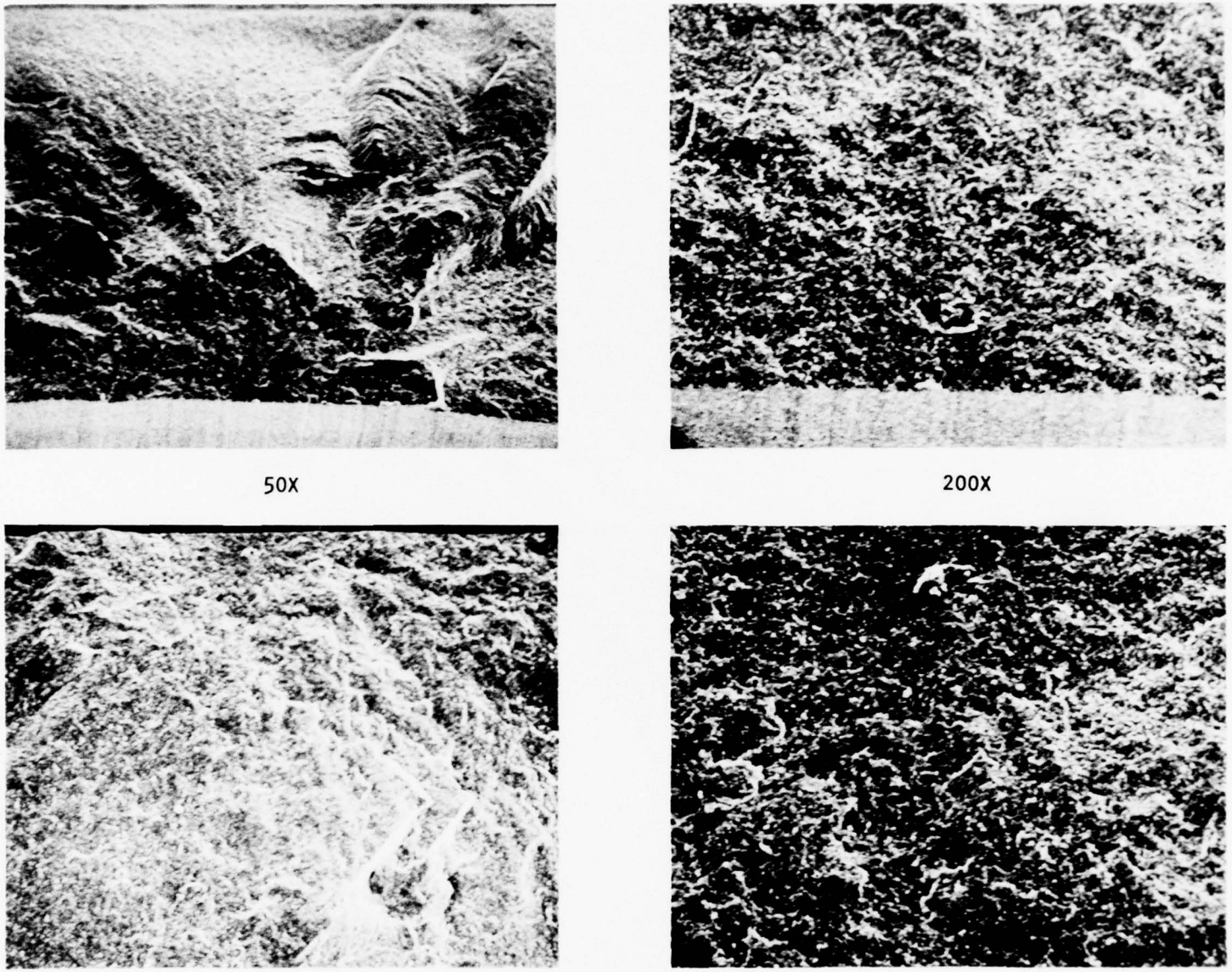


Figure 31. Fracture Surfaces of Ceralloy 147A Specimen 7 Showing Fracture Initiation Site.

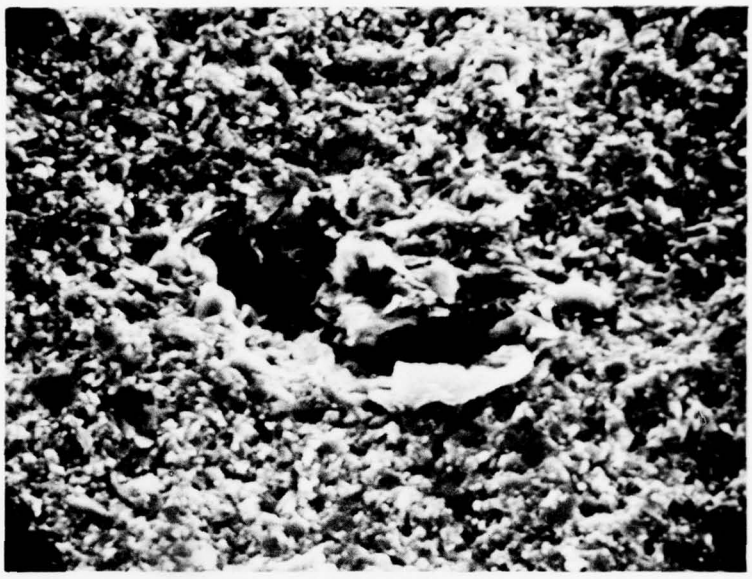

1000X

Figure 32. Fracture Initiation Site in Specimen 7 at High Magnification.

stayed in the other half. The defect is about 30 x 70 μm and consists of several unidentified flake-like crystals. Figure 33 shows one side of the fracture origin in specimen 10, which is located 0.4 mm off center and 10μm below the tensile surface. At 2000X it is seen to be an area of large crystals about 20 x 40 μm. Figure 34 shows one side of specimen 13. The mirror indicates the fracture origin is at or near the surface rather than at the defect that is present at a location that correlates well with the ultrasonic indication. The other side of the specimen shattered, so that the defect may have been lost as a result. It is therefore not clear whether or not this specimen failed as a result of the ultrasonically detected defect.

### 5.2.4 Correlation with Ultrasonic Results

Of the fifteen specimens tested, one was improperly machined and three others broke at low strengths at corner initiation sites. Of the remaining eleven, four appear to have failed at ultrasonically detected defects, two are uncertain and five appear to have failed from causes other than the ultrasonically detected defects. The defects measured were generally smaller than 100μm,which was expected since they gave ultrasonic reflections somewhat smaller than the seeded 125μm WC defect in the IDS. They were also located within the accuracies expected from the standard deviations of the measurement data, ±3200μm along the specimen length, ±2100μm along the specimen width and within ±480μm of the maximum measured depth plus 250μm. It should be noted that this last tolerance involves the necessary risk of machining away ultrasonically detected defects in an attempt to locate them near the tensile surface. These results are summarized in Table V.

## 5.3 NC-132 Hot Pressed Silicon Nitride

### 5.3.1 Specimen Preparation

Four of the six defects whose locations were measured were selected for flexural strength specimens. Three of these four defects were found to be surface pits and the fourth was identified by depth measurement as being close to the surface. The specimens were prepared in the same manner as the specimens of Ceralloy 147A, except that no material was machined from the tensile surface in order to avoid removing the defects. Figure 35 shows a layout of the specimens on the C-scan.

### 5.3.2 Flexural Strength

Table IV lists the flexural strength of each specimen, the distance of the fracture origin from the center along the length, and the pulse height of the ultrasonic signal from the defect. The average flexural strength of these specimens was 379±56 $MN/m^2$ (54.9±8.1 ksi). This low value is undoubtedly due to the unmachined surface, which contained many optically visible pits. Specimen 21 is the only one that definitely originated fracture at the ultrasonically detected defect. Specimen 22 initiated fracture from a corner,

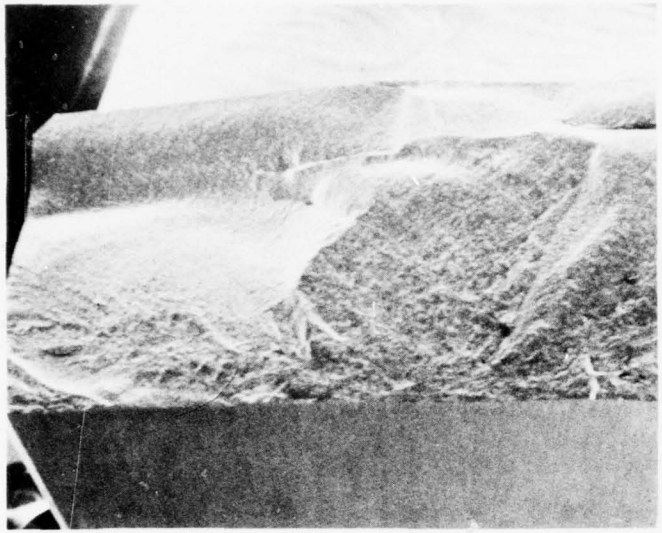

16X

1000X

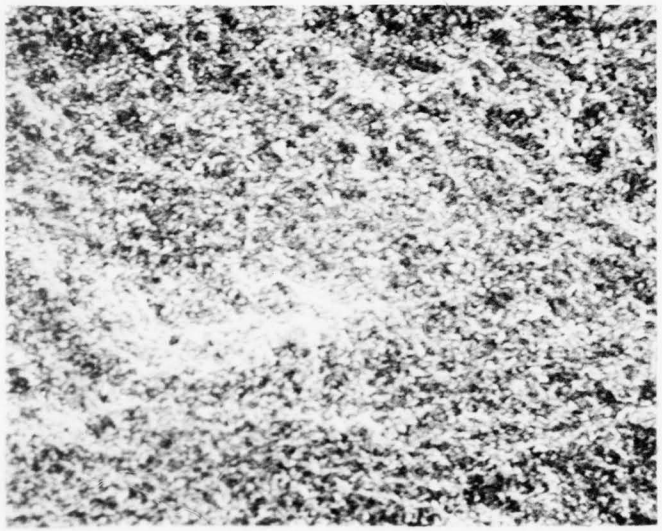

200X

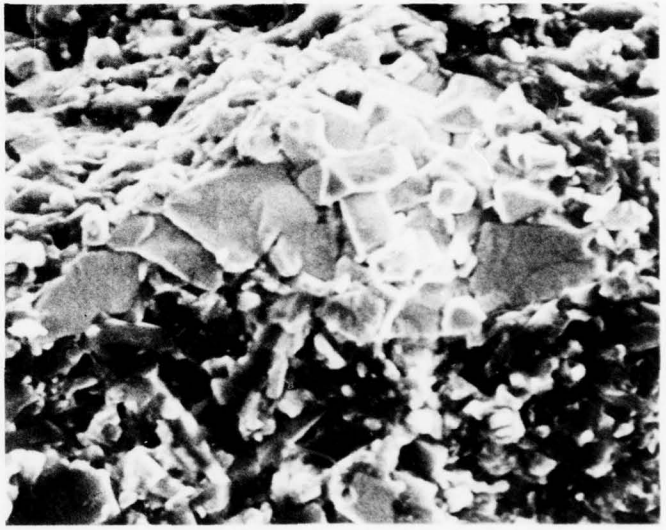

2000X

Figure 33. Fracture Surface of Ceralloy 147A Specimen 10 Showing Fracture Initiation Site.

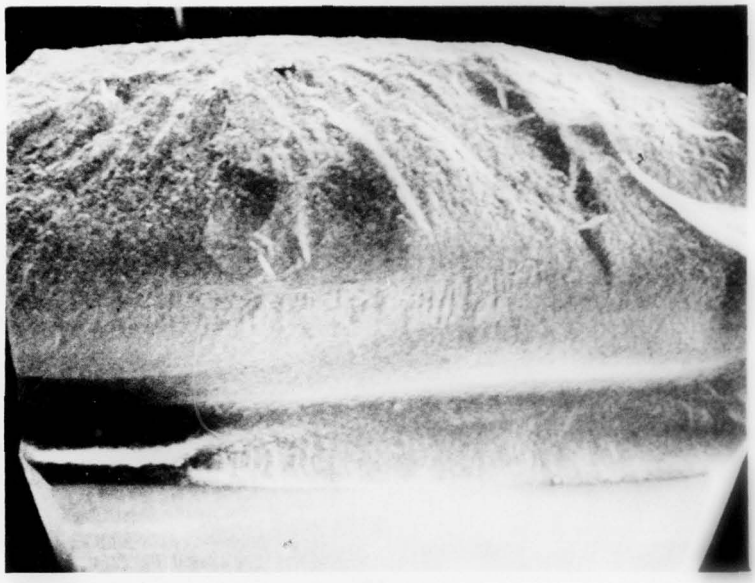

16X

50X

Figure 34. Fracture Surface of Ceralloy 147A Specimen 13.

TABLE V

ULTRASONIC CORRELATION DATA FOR HOT PRESSED SILICON NITRIDE

1. Ceralloy 147A

| Specimen No. | Flexural Strength $MN/m^2$ | Defect Size μm | Defect Location Off Center μm | Defect Location Depth μm | Comments |
|---|---|---|---|---|---|
| 3 | 191 | - | - | - | Fracture from site near corner |
| 8 | 388 | - | - | - | |
| 9 | 330 | - | - | - | |
| 2 | 683 | 100x40 | 1700 | 300 | inclusion |
| 6 | 619 | 40 to 80 deep | 1600 | 0 | crack |
| 7 | 636 | 70x30 | 0 | 60 | inclusion |
| 10 | 472 | 40x20 | 400 | 150 | inclusion |
| | Ave. 605±91 | | | | |
| 4 | 645 | ? | - | - | uncertain defect does not appear to be initiation site |
| 13 | 669 | 135x40 | 800 | 240 | |
| 1 | 717 | - | - | - | did not appear to fail at defect |
| 5 | 728 | - | - | - | |
| 11 | 733 | - | - | - | |
| 14 | 754 | - | - | - | |
| 15 | 771 | - | - | - | |
| | Ave. 741±22 | | | | |

2. NC-132

| | | | | | |
|---|---|---|---|---|---|
| 22 | 322 | - | - | - | corner |
| 21 | 367 | 200x100 | 120 | 0 to 100 | surface pit |
| 23 | 369 | - | - | - | uncertain |
| 24 | 456 | 30 deep | - | - | crack |

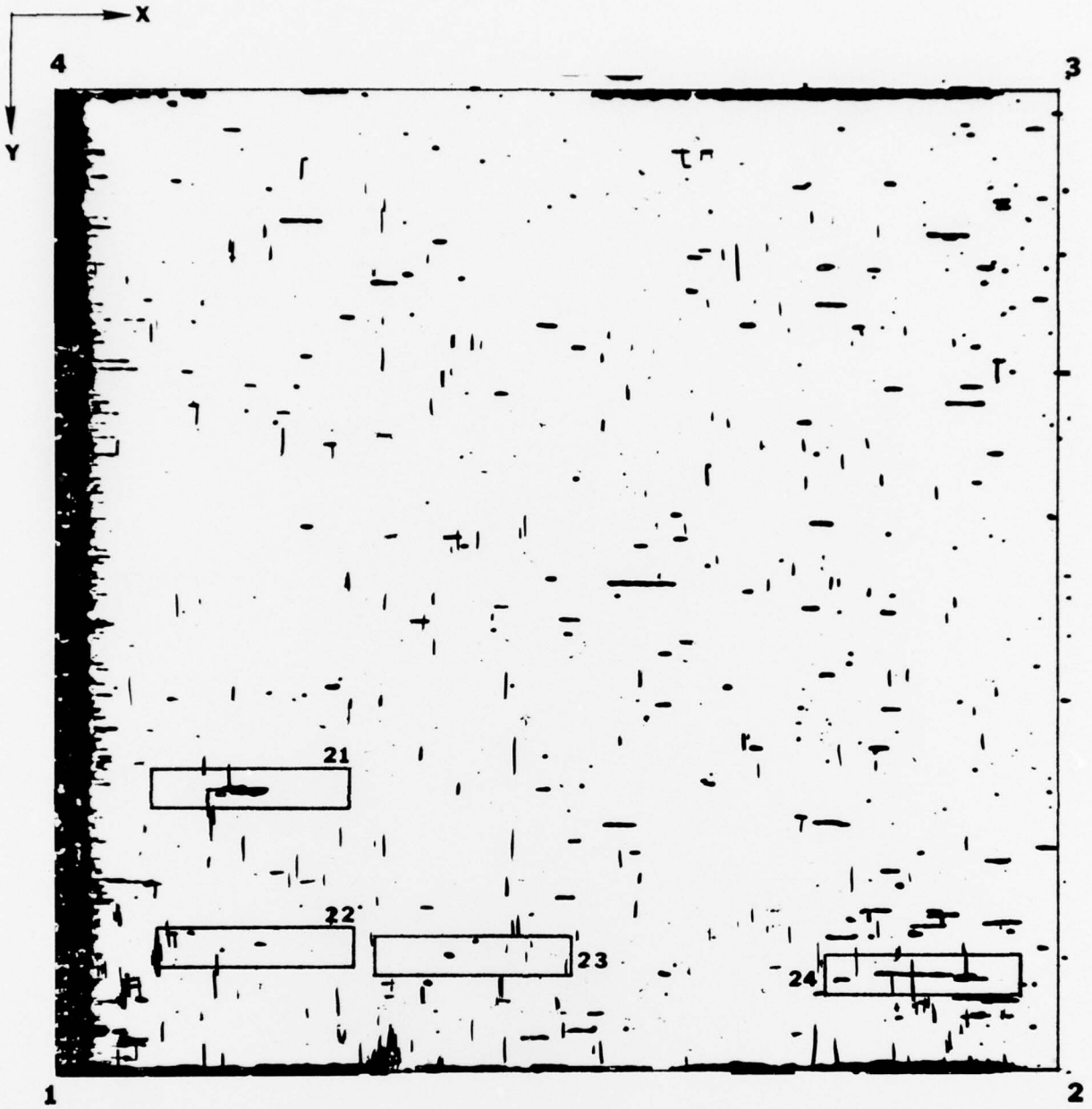


Figure 35. Specimen Locations in Billet of NC-132.

specimen 23 shattered, so that the fracture origin was lost and specimen 24 broke off center. In the case of specimen 24 the surface defect could be observed on one piece of the broken specimen well away from the fracture origin. There were not enough specimens of this material to draw any statistically significant conclusions, however, the general pattern of strengths versus types of failures was similar to the results for Ceralloy 147A.

### 5.3.3 SEM Fractography

Figure 36 shows the matching fracture surfaces of specimen 21 at 16 and 200X. The fracture origin in this specimen is definitely an ultrasonically detected surface pit about 200μm in diameter and 100μm deep. Figure 37 shows the matching fracture surfaces of specimen 22 at 16X, and also 200 and 500X views of the corner of the upper low magnification view. This figure shows a fracture which initiated near a corner and is typical of the appearance of the lowest strength specimens of both materials. In specimen 24, the failure initiated away from the shallow surface pit detected ultrasonically at the small surface defect shown in Figure 38. The higher magnification views of the fracture origin on the upper view of the matching fracture surfaces show a defect extending only about 30μm below the surface. This may be the side view of a small crack favorably oriented to cause specimen failure.

### 5.3.4 Correlation with Ultrasonic Results

Only specimen 21 of the four specimens of NC-132 tested broke through an ultrasonically detected defect. This defect was a surface pit of hemispherical shape that penetrated about 100μm. Since all of the defects in these specimens were in the same plane, the ultrasonic pulse heights should give a good indication of the relative defect sizes. The data in Table IV shows that specimen 21 had by far the largest signal. Therefore, the defects in the other specimens must have been much smaller, or at least shallower than 100μm. The defect in specimen 24 which caused failure was a 30μm deep, sharp defect which apparently had a higher stress concentration factor than the surface pit detected ultrasonically. This data indicates that it is important to develop the capability to detect sharp, small surface defects, such as the one in specimen 24, which apparently are too shallow to be detected by the shear wave technique. The results for these specimens are summarized in Table V.

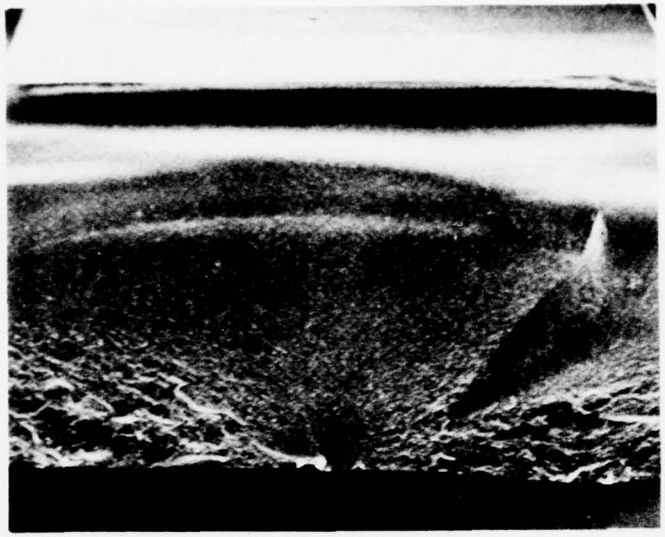

16X

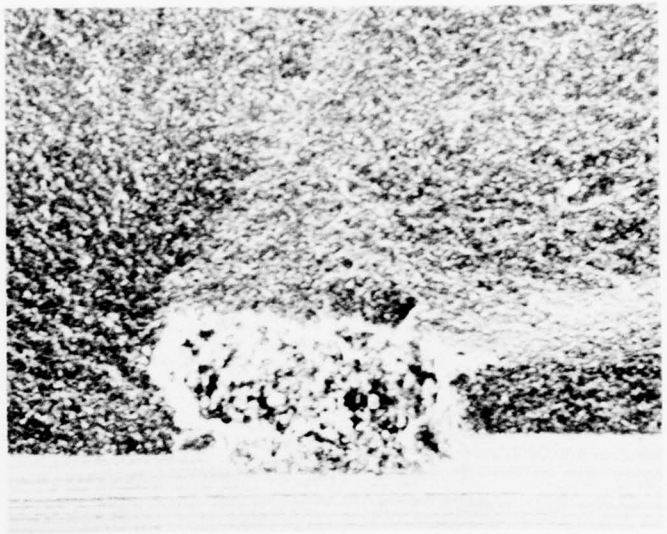

200X

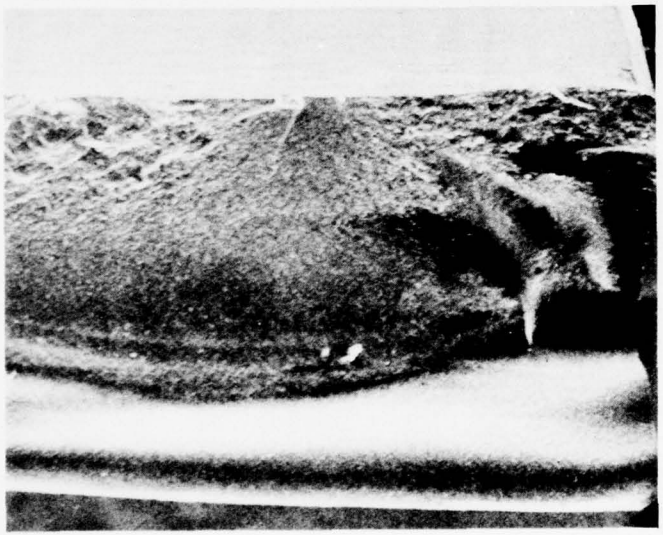

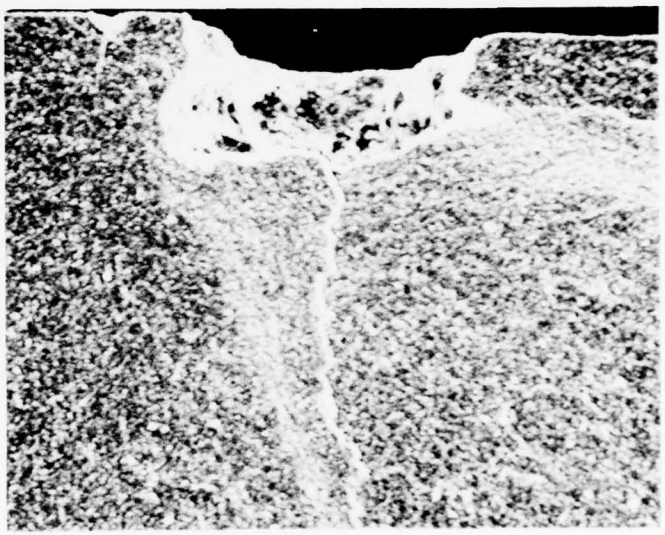

Figure 36. Fracture Surfaces of NC-132 Specimen 21 Showing Fracture Initiation Site.

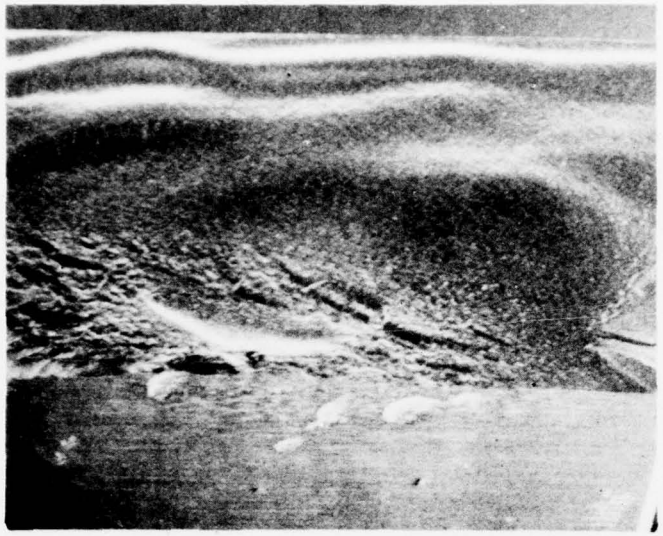

16X

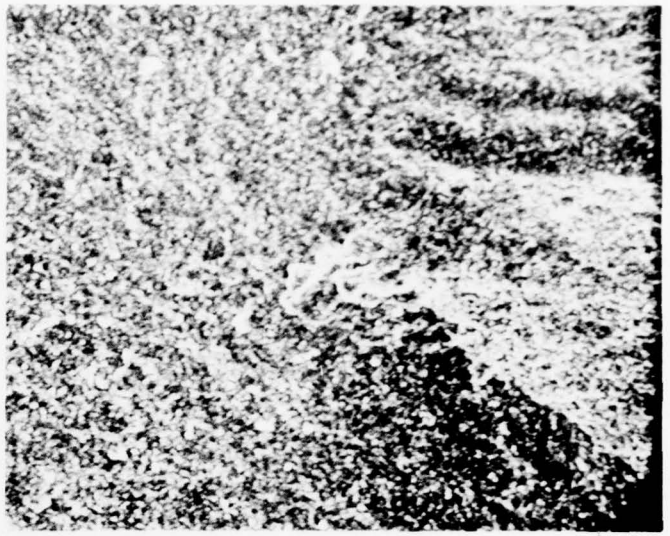

200X

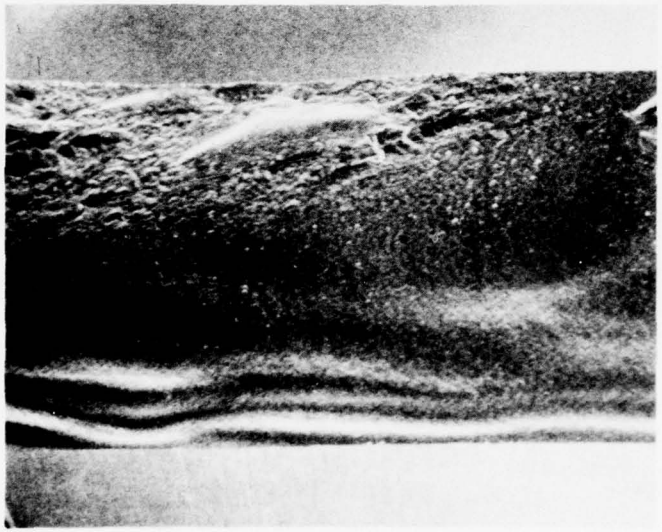

16X

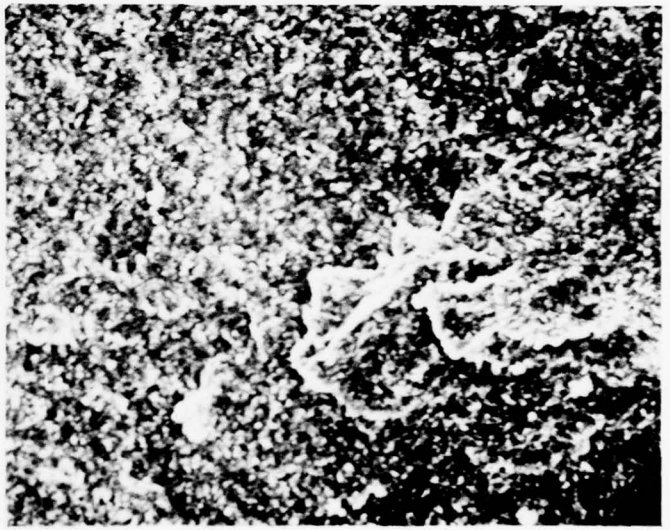

500X

Figure 37. Fracture Surfaces of NC-132 Specimen 22 Showing Typical Fracture Initiation From Corner.

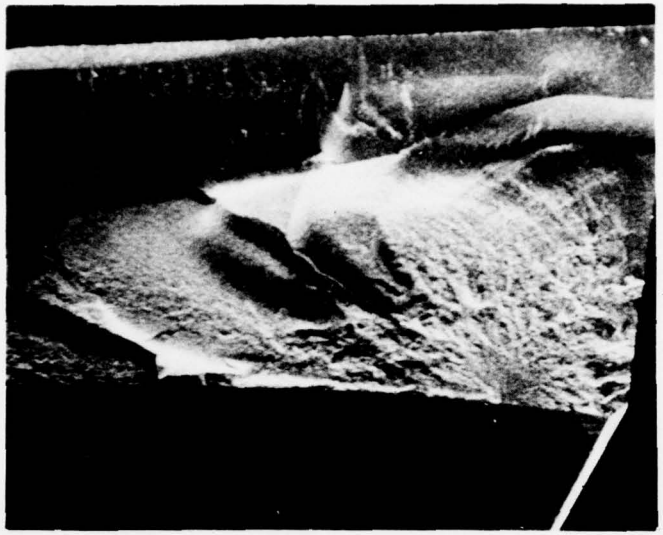

16X

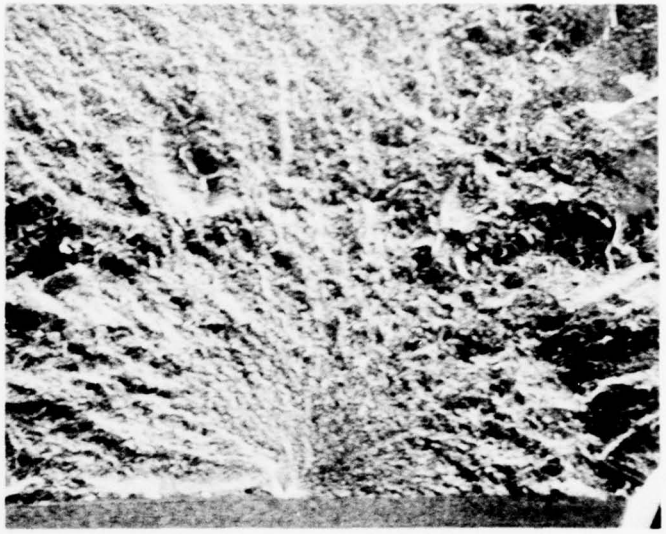

50X

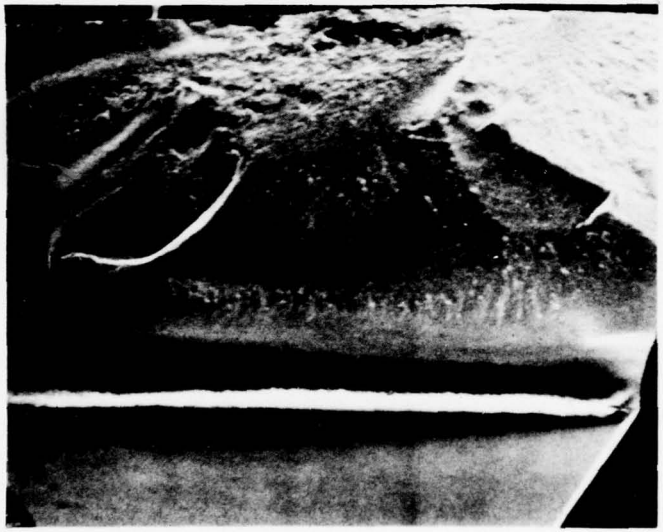

16X

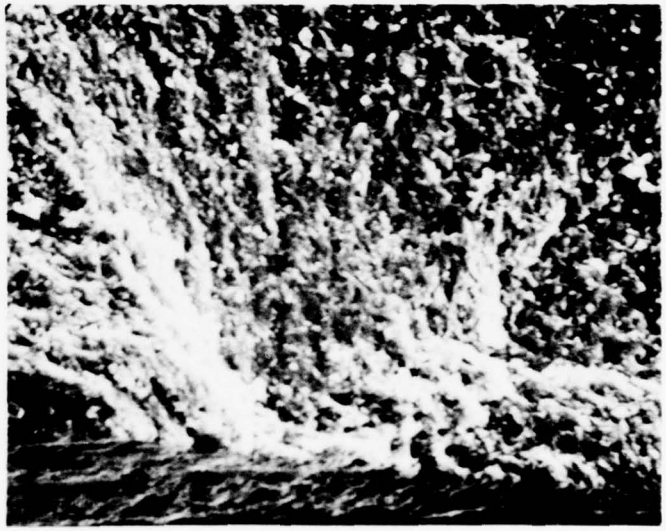

1000X

Figure 38. Fracture Surfaces of NC-132 Specimen 24 Showing Fracture Initiation Site.

## 6.0 CONCLUSIONS AND RECOMMENDATIONS

The purpose of this program is to develop high frequency ultrasonic evaluation techniques capable of detecting defects in the 10 to 100 μm (0.0004 to 0.004 inch) range. The specific objectives under this contract were to investigate ultrasonic evaluation at frequencies up to 75 MHz, to develop an ultrasonic shear wave technique and then to investigate the correlation of the results of evaluations using this technique with flexural strength.

Investigation of the ultrasonic evaluation effort covered frequencies up to 75 MHz. The best results achieved were at 45 MHz. While this seems to contradict theory, it is the result of the bandwidth-sensitivity characteristics of the instrumentation/transducer that were in use in the experiments. The development of a high-frequency ultrasonic system having satisfactory bandwidth-sensitivity characteristics for up to 100 MHz is strongly recommended. This would allow utilization of the advantages expected to be gained from higher frequency inspection methods. It is also recommended that computerized data storage and diagnosis be developed to replace the time consuming analysis required by the use of C-scan recording.

In spite of the frequency limitations noted above, a 45 MHz ultrasonic shear wave technique was successfully developed, which was found to be more sensitive than the 45 MHz longitudinal wave technique previously developed. This improved sensitivity is attributed to the lower ultrasonic velocity of shear waves, which yields a shorter wavelength for detection of smaller defects. The shear wave technique (due to its different ultrasonic wave mode and beam orientation) was also found to be relatively more sensitive for detection of defects oriented preferentially to cause failure. A comparison of flexural strength data in nine specimens of Ceralloy 147A led to the conclusion that, at the 90% confidence level, the four specimens that broke through defects detected by the ultrasonic shear wave technique were significantly weaker than the five specimens which failed with no such defect as the initiation site. Comparative average strengths are 605 and 741 $MN/m^2$ (87.7 and 107.4 ksi). The defects involved had major dimensions of 40 to 100 μm (0.0016 to 0.001 inch).

Preliminary evaluations of artificial surface defects indicate that defects that do not extend at least 40 μm (0.0016 inches) below the surface are not detected by the shear wave technique. For detection of these small surface defects it is recommended that ultrasonic surface wave inspection be investigated.

## 7.0 REFERENCES


1. Derkacs, T., Matay, I.M., and Brentnall, W.D., "Nondestructive Evaluation of Ceramics," Final Technical Report, Contract N00019-75-C-0238, Naval Air Systems Command, July, 1976.

2. Private communication from J. A. Rubin, Technical Director, Ceradyne, Inc., January 13, 1977.

3. Private communication from C. A. Johnson, General Electric Co. Research and Development Center, May 18, 1976.

4. Petrovic, J.J., et al, "Controlled Surface Flaws in Hot-Pressed $Si_3N_4$," J. Am. Ceram. Soc., Vol. 58, Nos. 3 and 4, 1975, pp. 113-16.

5. Harrison, D.E., "Properties Important to the Design of Ceramic Stator Vanes for Indust ial Gas Turbines," Proc. British Ceramic Soc., No. 22, 1973, pp. 391-408.

6. Fate, W.A., "High Temperature Shear Modulus of $Si_3N_4$ and SiC," J. Am. Ceram. Soc., Vol. 57, No. 1, Jan., 1974, pp. 49-50.

7. Rosinger, H.E., Ritchie, J.G., and Shillinglau, A.J., "A Systematic Study of the Room Temperature Elastic Moduli of Silicon Carbide," Materials Science and Engineering, 16, 1974, pp. 143-154.

8. Hicks, C.R., "Fundamental Concepts in the Design of Experiments," Holt, Rinehart and Winston, N.Y. 1964, pp. 12-14.

9. Baumgartner, H.R. and Richerson, D.W., "Inclusion Effects on the Strength of Hot Pressed $Si_3N_4$," Fracture Mechanics of Ceramics, Vol. 1 Concepts, Flows and Fractography, Edited by R. C. Bradt, et al., Plenum Press, NY, 1974, pp. 367-386.

## DISTRIBUTION

(one copy unless otherwise noted)

(3 copies plus balance after distribution)
U. S. Naval Air Systems Command
AIR-52031B
Department of the Navy
Washington, D.C. 20361

(7 copies, for internal distribution by AIR-954)
AIR-954 (2 copies), AIR-5361B1 (1 copy), AIR-330A (1 copy)
AIR-330B (1 copy), AIR-5361A (1 copy), AIR-5362A (1 copy)
U. S. Naval Air Systems Command
AIR-954
Department of the Navy
Washington, D.C. 20361

(2 copies)
Commander
Naval Air Development Center
Code 302A, A. Fletcher (1 copy), Code 30232, W. Scott (1 copy)
Warminster, Pennsylvania 18974

(2 copies)
U. S. Naval Air Turbine Test Station
Attn: J. Glatz (PE-43) (1 copy) A. Martino (AT-1) (1 copy)
1440 Parkway Avenue
Trenton, New Jersey 08628

U.S. Naval Sea Systems Command
(ORD-035)
Department of the Navy
Washington, D.C. 20362

Commander
Naval Weapons Center
Code 5516
China Lake, California 93555

Naval Ships Engineering Center
Code 6146
Center Bldg. Room 202
Prince Georges Center
Hyattsville, Maryland 20782

## DISTRIBUTION

Naval Surface Weapons Center
Attn: W. Mannschreck
Dahlgren, Virginia 22448

U.S. Naval Ships Research and Development Center
Code 2812
Annapolis, Maryland 21402

Naval Surface Weapons Center
(Metallurgy Division)
White Oak
Silver Spring, Maryland 20910

(2 copies)
Director
Naval Research Laboratory
Code 6400 (1 copy)
Code 6360 (1 copy)
Washington, D.C. 20375

Office of Naval Research
The Metallurgy Program, Code 471
Arlington, Virginia 22217

(2 copies)
Director
Army Materials and Mechanics Research Center
A. Gorum (1 copy), G. A. Darcy, Jr. (1 copy)
Watertown, Massachusetts 02171

Commander, U.S. Army Material Command
Attn: AMCRD-TC
5001 Eisenhower Avenue
Alexandria, Virginia 22304

U. S. Army Aviation Material Laboratories
Fort Eustis, Virginia 23604

(2 copies)
Air Force Materials Laboratory
Code LLM (1 copy) Code LL (1 copy)
Wright-Patterson Air Force Base
Dayton, Ohio 45433

## DISTRIBUTION

Air Force Propulsion Laboratory
Code TBP
Wright-Patterson Air Force Base, Ohio 45433

National Aeronautics and Space Administration
Code RWM
Washington, D.C. 20546

(3 copies)
National Aeronautics and Space Administration
Lewis Research Center
C. M. Ault (1 copy)
H. P. Probst (1 copy)
W. A. Sanders, MS 49-1 (1 copy)
21000 Brookpark Road
Cleveland, Ohio 44135

U.S. Energy Research and Development Administration
Division of Reactor Development
(A. Van Echo)
Washington, D.C. 20545

Metals and Ceramics Information Center
Battelle Columbus Laboratories
505 King Avenue
Columbus, Ohio 43201

The Johns Hopkins University
Applied Physics Laboratory
(Maynard L. Hill)
Johns Hopkins Road
Laurel, Maryland 20810

AVCO RAD
201 Lowell Street
Wilmington, Massachusetts 01887

ITT Research Institute
10 West 35th Street
Chicago, Illinois 60616

## DISTRIBUTION

Detroit Diesel Allison Division
General Motors Corporation
Materials Laboratories
Indianapolis, Indiana 46206

Pratt and Whitney Aircraft
(Mr. A. Magid)
Florida Research and Development Center
West Palm Beach, Florida 33402

Chief, Materials Engineering Department
Dept. 93-39M
AiResearch Manufacturing Co. of Arizona
402 South 36th Street
Phoenix, Arizona 85034

Lycoming Division
AVCO Corporation
Stratford, Connecticut 06497

Curtis Wright Company
Wright Aeronautical Division
Wood-Ridge, New Jersey 07075

Bell Aerosystems Company, Technical Library
P.O. Box 1
Buffalo, New York 14140

General Electric Company
Aircraft Engine Group
Materials and Processes Technology Laboratories
Evendale, Ohio 45215

Solar
(Dr. A. Metcalfe)
2200 Pacific Highway
San Diego, California 92112

Teledyne CAE
1330 Laskey Road
Toledo, Ohio 43601

Stellite Division
Cabot Company
Technical Library
P.O. Box 746
Kokomo, Indiana 46901

## DISTRIBUTION

(2 copies)
General Electric Co.
Corporate Research and Development
Attn: W. Hillig (1 copy)
R. Charles (1 copy)
Schenectady, New York 12301

Norton Company
Protective Products Division
(N. J. Ault)
Worcester, Massachusetts 01606

Westinghouse Electric Company
Materials and Processing Laboratory
(Ray Bratton)
Beulah Road
Pittsburgh, Pennsylvania 15235

Westinghouse Electric Company
Lester Branch 9175
(A. N. Holden)
Philadelphia, Pennsylvania 19113

Research Library and Development Division
The Carborundum Company
P.O. Box 337
Niagra Falls, New York 14302

Ford Motor Company
Product Development Group
(E. A. Fisher)
2000 Rotunda Drive
Dearborn, Michigan 48121

General Electric Company
AEG Technical Information Center
Mail Drop N-32, Bldg. 700
Cincinnati, Ohio 45215

Professor Richard E. Tressler
Ceramic Science Section
Pennsylvania State University
201 Mineral Industries Bldg.
University Park, Pennsylvania 16802

## DISTRIBUTION

Dr. T. D. Chikalla
Ceramics and Graphite Section
Battelle - Northwest Laboratories
Richland, Washington 99352

United Aircraft Research Laboratories
East Hartford, Conn. 06108

Pratt & Whitney Aircraft
East Hartford, Connecticut 06108

Deposits and Composites, Inc.
1821 Michael Faraday Drive
(R. E. Engdahl)
Reston, Virginia 22090

Oak Ridge National Laboratory
Post Office Box 4
(R. W. McClung)
Oak Ridge, Tennessee 37830

SKF Industries
(Harish Dalal)
1100 First Avenue
King of Prussia, Pennsylvania 19406

North American Rockwell Science Center
P.O. Box 1085
1049 Camino Dos Rios
Thousand Oaks, California 91360

FINAL REPORT ONLY (12 copies for DDC)
Commander
Naval Air Development Center
Code 302A, A. Flectcher
Warminster, Pennsylvania 18974

FINAL REPORT ONLY (3 COPIES)
Commander, Naval Air Development Center
Code 813
Warminster, Pennsylvania 18974